Pressure Dependence of Polymer Fluids: Application of the Lattice Cluster Theory

Jacek Dudowicz and Karl F. Freed*

The James Franck Institute and the Department of Chemistry, University of Chicago, Chicago, Illinois 60637

Received March 20, 1995; Revised Manuscript Received July 3, 1995[⊗]

ABSTRACT: The lattice cluster theory is used to analyze the pressure dependence of the effective Flory interaction parameter χ_{eff} observed in recent small-angle neutron scattering experiments for polymer blends. A description of this pressure dependence in blends requires a theory that contains a minimum of four empirical parameters, three interactions energies and one lattice cell volume, a set smaller than in the seven- or eight-parameter treatments generally employed with other methods. The conventional liquid mixture philosophy is used for determining this minimal set of parameters as follows: The self-interaction parameters and pure component cell volumes are obtained from fits to pure melt *PVT* data. A common combining rule then provides the blend cell volume as functions of those for the pure melts, but the common geometric combining rule for the heterocontact interaction energy is found to be grossly inadequate. Hence, this interaction parameter is chosen by fitting to blend data. Explicit comparisons with experimental data for polystyrene (PS) and poly(vinyl methyl ether) (PVME) melts, PS/PVME blends, and PS-*b*-PMMA (poly(methyl methacrylate)) diblock copolymers demonstrate that this minimal lattice cluster theory provides a good representation of melt equations of state, the composition, temperature, molecular weight, and pressure dependence of the small-angle neutron scattering, the composition dependence of the volume change on mixing, the spinodal curves, and the composition and temperature dependence of the blend correlation length. Additional predictions are presented concerning the stabilization and destabilization of blends by diblock copolymers.

I. Introduction

One factor stimulating the rapid growth of small-angle neutron scattering (SANS) experiments is the ability of extracting the Flory effective interaction parameter χ_{eff} from the experimental data. This parameter is of interest for use in predicting the behavior of several thermodynamic properties of polymer systems. The χ_{eff} parameter has also been endowed with a microscopic interpretation through the Flory–Huggins formula[1] for χ^{FH}.

Classic Flory–Huggins theory[1] for an incompressible binary polymer blend leads to the equation

$$\chi^{FH} = z(\epsilon_{11} + \epsilon_{22} - 2\epsilon_{12})/(2k_BT) = z\epsilon/(2k_BT) \qquad (1.1)$$

where z is the number of nearest neighbors to a lattice site, k_BT is the thermal energy, and the $\{\epsilon_{\alpha\beta}\}$ are attractive nearest neighbor van der Waals energies between monomers of species α and β. The Flory–Huggins theory[1] predicts χ^{FH} as being inversely proportional to temperature and as being independent of composition, molecular weights, chain architectures, and pressure. Unfortunately, all of these latter predictions from eq 1.1 conflict with a wide body of experimental data, indicating serious deficiencies in Flory–Huggins theory despite its widespread application and the general belief in its veracity because of its extensive use in fitting and correlating data. Further evidence for severe inherent errors of Flory–Huggins theory emerges from Monte Carlo simulations[2,3] of the identical lattice model used initially to derive Flory–Huggins theory. These simulations are important because they provide exact numerical solutions of the lattice model. Hence, comparisons between theory and simulation are not marred by the presence of adjustable parameters. The no-parameter comparisons indicate[2,3] gross errors, with factors of roughly 2 discrepancies in the Flory–Huggins prediction of the critical temperature for a polymer–solvent system as well as serious errors in the heats and entropies of mixing.

While it is clear that more realistic theories are needed to describe polymer systems, several different approaches are necessary to provide complementary information about these rather complex systems. Full atomistic potential treatments require very extensive computer simulations to generate specific numbers for a very particular system. The values of these numbers are, however, dependent on the quality of the empirical potential functions, the neglect of three-body interactions, etc. More importantly, the computer simulations provide experimentally unavailable microscopic information[4] for use in testing, refining, and developing improved theories of the polymer systems. Another approach[5–7] employs more simplified hard-core or Lennard-Jones models for the monomer–monomer interactions in conjunction with, for instance, liquid state theories to gain an overall understanding for various generic behaviors of polymer melts and blends. The oversimplicity of hard-core and Lennard-Jones monomer–monomer interaction models is but one reminder that these theories must likewise have limitations in their applicability to specific polymer systems. Nevertheless, their utility lies in their relative ease of application (compared to full atomistic simulations) and the generality of many of their predictions.

A further simplification is afforded by using the less realistic lattice models because these models enable the development[8–11] of single analytical expressions governing a wide range of systems and molecular parameters, a feature enabling the use of the theory, for instance, to map out the complex constant-pressure phase diagrams of ternary polymer systems, something which would become computationally prohibitive with the other two theoretical approaches. The mathematical simplicity of lattice models is partially offset by a more

[⊗] Abstract published in *Advance ACS Abstracts,* September 1, 1995.

0024-9297/95/2228-6625$09.00/0

approximate representation of reality, but recent advances with the lattice cluster theory[11] (LCT) have enabled the consideration of a generalized lattice model[9] in which monomers are endowed with specific molecular structures by permitting them to extend over several lattice sites. Thus, the generalized lattice model provides a molecular representation intermediate in character between that of full atomistic potential simulations and that of theories with hard-sphere or Lennard-Jones models for the monomers. This molecular representation of the LCT is useful for probing, among other things, the influence of monomer size, shape, and structure and of chain architecture on the physical properties of polymer systems.

There is a huge leap taken when model-based theories are used to explain experimental data for such complex systems as polymer fluids. The above-noted limitations to the various types of models imply that even if the models are solved rather accurately, they must be deficient in representing certain aspects of the real systems. Some of these deficiencies are, perhaps, swept under the rug by the adjustment of parameters to fit experimental data. A more severe test for the utility of the theory emerges only upon its use to explain a wide variety of fundamentally different experimental data by employing a small common set of adjustable parameters. When a theory survives such a stringent test, we should still be extremely cautious in literally believing the underlying model, because any model of polymer systems must have limitations. Rather, the model should be tested further to uncover its failures, to suggest further improvements of the model, and to understand the ranges over which the successful fits to experimental data may be used safely for predictive purposes.

The philosophy described in the previous paragraph has motivated our extensive comparisons of lattice cluster theory predictions with a wide variety of experimental and simulation data for polymer blends. Our computations[12-14] indicate that the specific monomer structures play a significant role in determining the composition dependence of the observed Flory interaction parameter χ_{eff} and in producing the entropic contribution to χ_{eff}. Other relevant features involve the presence of local correlations, which are induced by packing constraints and interactions (nonrandom mixing). Important contributions emerge also from the so-called "equation of state effects", the variation of polymer properties with thermodynamic state and, in particular, with pressure. While it has been customary to describe polymer melts and blends as being incompressible, our LCT computations[12-14] have predicted important influences of "compressibility", i.e., from the fact that these systems are not incompressible. This outlook has begun to be incorporated into other theoretical approaches[15] and has stimulated recent experimental determinations[16,17] of a nontrivial pressure dependence to SANS experiments for polymer blends. This observed[16,17] pressure dependence, predicted[12] by the LCT before the experiments, in turn, provides a wealth of new experimental data for comparison with the LCT predictions in order to test, refine, and understand the applicability of the LCT to real polymer blends.

Confronting the pressure-dependent SANS data for polymer blends first requires testing whether the LCT provides an adequate representation to the pressure dependence of blend thermodynamics. Since *PVT* data are generally unavailable for polymer blends, this test must rely on descriptions of the more available *PVT* properties for the pure component melts. However, theoretical treatments of liquid mixtures traditionally begin by fitting the pure component parameters to experimental data. The mixtures are then described using various combining rules for the binary system parameters. Thus, we begin here by comparing the LCT equation of state for polymer melts with experimental *PVT* data. Several other treatments[18,19] exist for the polymer melt equation of state, and the customary procedure is based on determining the parameters from a least squares fit to the pressures. This procedure weights significantly more heavily the highest pressure data, while the majority of the available SANS data applies to lower pressures. Thus, we seek only an adequate theoretical description over the modest pressure range of roughly 1000 atm. In fact, previous approaches generally also display defficiencies over large pressure regions, so parameters are chosen separately for narrower ranges of temperature and pressure.[20] Whereas these previous theoretical treatments[18,19] of melt *PVT* properties employ three (or even more) adjustable parameters for each pure substance, we describe the limited pressure range with only two microscopic parameters, the interaction energy ϵ_{ii} and the volume $v_{\text{cell}}^{(i)}$ associated with a single lattice site. Improved descriptions over wider pressure ranges should be possible by the addition of a third adjustable parameter, but we retain the two-parameter approach to minimize the proliferation of parameters. By contrast, the earlier treatments[19,21,22] would contain three pure component parameters (T^*, P^*, and ϱ^*) for each substance, plus one or two interaction parameters (depending on whether separate entropic and enthalpic components are used). These seven- or eight-parameter approaches are still generally deficient in describing the composition dependence of the Flory effective interaction parameter χ_{eff}. Thus, our more molecularly oriented theory is designated to describe polymer blends with a considerably reduced set of adjustable parameters.

The transition to describing polymer blends requires the introduction of a combining rule for the pure component cell volumes since the lattice model does not prescribe the choice of these parameters for mixtures. We attempt to choose monomer structures such that the cell volumes are as similar as possible, but our use of a cubic lattice emphasizes the modelistic nature of the theory and the fact that exact equality is not possible for the pure component cell volumes. Combining rules are not employed, on the other hand, for the blend heterocontact interaction energy ϵ_{12} because their use would introduce gross errors into the prediction of blend properties as is understood even using simplistic Flory–Huggins theory. The ϵ in eq 1.1 represents a small quantity that is the difference between two rather large energies, $\epsilon_{11} + \epsilon_{22}$ and $2\epsilon_{12}$. A 1% deviation of ϵ_{12} from, for instance, the popular geometric combining rule of $\epsilon_{12} = (\epsilon_{11}\epsilon_{22})^{1/2}$ could represent a 100% shift in ϵ and hence in the critical temperature. Thus, the parameter ϵ_{12} must be determined empirically from fits to experimental data. Lacking extensive data for *PVT* blend properties, the ϵ_{12} is fit to SANS data for blends. This analysis begins to address the question posed to us by some experimentalists as to the necessary experimental data for determining the parameters in the simplest versions of the LCT model for polymer blends. The traditional approach, taken in theories of mixtures,

appears adequate, namely, fitting pure component parameters to data for the pure components and then determining the residual ϵ_{12} from some data for the mixture.

The applications presented here focus upon the polystyrene/poly(vinyl methyl ether) (PS/PVME) system because this is the blend for which the pressure-dependent SANS data[16,17] are available and also because there are rather extensive 1 atm SANS data[23] for this system and considerable *PVT* data[24] for PS melts. Our previous treatment[13] of the 1 atm SANS data for PS/PVME blends is more concerned with understanding the relevance of including monomer structures and blend compressibility in theories of the SANS χ_{eff} parameter. Thus, the previous work[13] does not consider the tedious simultaneous description of the pure component *PVT* data treated here. The same set of parameters is used here for describing the *PVT* data of the pure components as is used to reproduce data for the volume change on mixing ΔV, the SANS interaction parameter χ_{eff}, the spinodal curves, and the correlation lengths ξ for the blends.

Section II briefly defines the generalized lattice model for various polymer systems (pure melts, binary A/B blends, A-*b*-B diblock copolymer melts, or ternary A/B/A-*b*-B polymer mixtures) and outlines the theoretical background of the lattice cluster theory. We briefly describe the method of generating the Helmholtz free energy for the above systems as well as an altered LCT procedure for calculating the SANS effective interaction parameter for binary blends and diblock copolymer melts. This procedure involves the direct theoretical computation of the absolute scattering intensities $I(0)$ without the common need for introducing an arbitrary chosen normalizing volume v_0 as appears in common definitions of χ_{eff}. The resultant treatment evaluates the LCT χ_{eff} and the experimental χ_{eff} in an identical fashion from $I(0)$ [or $I(q^*)$ for block copolymers]. Section II also discusses a modified expression for the volume change on mixing to account for the different cell volumes for the pure components, a difference ignored, for simplicity, in our earlier LCT calculations.[13]

The LCT computations and extensive comparisons with experiments are summarized in section III. The comparisons begin with the *PVT* properties for pure PS and PVME melts. The computed properties for the binary PS/PVME blends include the effective interaction parameter χ_{eff}, the spinodal curves, the correlation lengths ξ, the excess volume V^e, and the pressure dependence of SANS data (such as χ_{eff}, $I(0)$, etc.). The LCT computations for diblock copolymers are illustrated by comparison with experiment[25,26] for the temperature dependence of χ_{eff} for PS-*b*-PMMA diblock copolymer melts. Section IV summarizes the main conclusions and analyzes the spinodal curves for the ternary PS/PVME/PS-*b*-PVME system (even though PS-*b*-PVME diblocks have not yet been synthesized). This analysis is designed to demonstrate the general utility of the LCT for predicting the interesting phase behavior of complex ternary polymer mixtures. Readers more interested in the LCT predictions and in the extensive comparison with experiment may skip directly to section III.

II. Lattice Cluster Theory of Polymer Fluids

A. Generalized Lattice Model of Polymer Fluids. The generalized lattice model depicts a k-component polymer system by a set of $n = \sum_{i=1}^{i=k} n_i$ polymer chains placed on a regular array of N_l lattice sites and

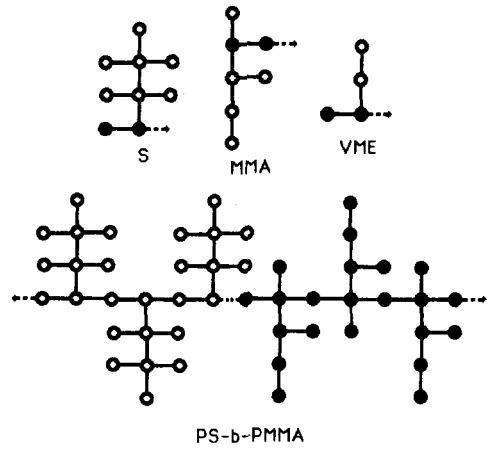

Figure 1. Models of the monomer structures used for styrene (S), methyl methacrylate (MMA), and vinyl methyl ether (VME) as well as the single-bond model of the junction structure in a PS-*b*-PMMA diblock copolymer chain. Circles denote monomer portions that occupy single lattice sites, and lines depict bonds that are assumed to be fully flexible in three dimensions. Solid circles represent monomer portions belonging to the backbone chain, and arrows indicate the directions of linkages between monomers to form homopolymer chains or block copolymers.

coordination number z. Each monomer of a given species α (α = A, B, C, ...) has a specified molecular structure and occupies s_α lattice sites. There is no restriction concerning the number of species in the systems. However, because the present calculations are performed for pure melts, A-*b*-B diblock copolymer systems, A/B binary blends, and A/B/A-*b*-B ternary mixtures, we consider only α = A and B in order to keep the notation compact. The structures for the A and B monomers are chosen, whenever possible, as those most closely corresponding to united atom models in which the united atom groups, such as CH_n, residue at single lattice sites. Figure 1 displays examples of the monomer architectures used in our calculations and also presents the model of a typical diblock copolymer chain with structured monomers. The junction between the two blocks in a copolymer molecule is assumed to be provided by a single bond (the dashed line in Figure 1), but other junction models may be treated as well. All homopolymer and copolymer bonds in the system are taken as fully flexible in three dimensions, and all chains are assumed to be monodisperse, for simplicity.

Each homopolymer chain of species α has N_α monomers and extends over $M_\alpha = N_\alpha s_\alpha$ lattice sites, while the analogous chain occupancy index M_{AB} for the A-*b*-B diblock copolymer emerges as the sum of contributions from its two blocks, i.e., $M_{AB} = N_A^{(b)} s_A + N_B^{(b)} s_B$, where $N_\alpha^{(b)}$ is the polymerization index for block α. Liquid state polymer systems are compressible fluids as evidenced by their nontrivial equations of state and other well-known thermodynamic implications. We have stressed[13,27-29] the importance of including blend (or diblock copolymer melt) "compressibility" even in the analysis of experimental SANS data. This polymer fluid compressibility is introduced into the generalized lattice model by allowing n_v lattice sites to be empty. The void volume fractions $\phi_v = n_v/N_l$ are determined from the appropriate equation of state for a given polymer system. The resultant ϕ_v for blends requires specifying the blend composition Φ_1 (or a set of compositions $\{\Phi_i\}$ for the general multicomponent case). The composition of such a compressible k-component polymer mixture is expressed in terms of either the actual volume

fractions $\phi_i = n_i M_i/N_l$ (normalized as $\sum_{i=1}^{i=k}\phi_i + \phi_v = 1$) or the nominal volume fractions $\Phi_i = \phi_i/(1 = \phi_v)$ satisfying the condition $\sum_{i=1}^{i=k}\Phi_i = 1$. The latter composition variables are most closely related to the experimental volume fractions $\Phi_i^{(exp)} = V_i/\sum_{i=1}^{i=k}V_i$, where V_i denotes the volume of pure component i. The equation of state then produces ϕ_v as a function of temperature, pressure, composition $\{\Phi_i\}$, and the volume v_{cell} of a unit cell on the lattice.

The lattice is assumed to be a three-dimensional ($d = 3$) cubic lattice with $z = 2d = 6$. The unit cell volume v_{cell} associated with each lattice site is treated as an adjustable parameter. The computations in section III determine the pure component $v_{cell}^{(melt)}$ from fits to PVT data, while the v_{cell} for multicomponent systems are defined in section III by using common combining rules.

The interactions in fluids involve short-range repulsions and longer range attractions. While the former are naturally represented in the lattice model by the excluded volume constraints that prohibit multiple occupancy of lattice sites, the latter are introduced by ascribing attractive microscopic van der Waals energy $\epsilon_{\alpha\beta}^{ij}$ to nearest neighbor (on the lattice) portions i and j of monomers α and β. For simplicity, all s_α portions of a monomer α are taken as energetically equivalent units, which interact with the same energies $\epsilon_{\alpha\beta}$. While the LCT can be applied with different interaction energies for the different united atom portions of each monomer and while such a set of interactions is physically sensible, our use of monomer-averaged interactions is designated to *minimize* the number of adjustable parameters until we find enough experimental data *requiring* the introduction of a larger set of interaction parameters. This simplification in describing the interaction energies leads for compressible binary blends or for diblock copolymer systems to the presence of three independent interaction energies ϵ_{AA}, ϵ_{BB}, and ϵ_{AB} which are fit to experimental data. Pure melt data provide the input for determining the single-component ϵ_{AA} and ϵ_{BB}. As described in section III, combining rules are inadequate in generating suitable values for ϵ_{AB}, so ϵ_{AB} is instead obtained using experimental data for binary blends[23] or diblock copolymers.[25,26] As noted above, combining rules do appear to suffice for estimating the cell volume $v_{cell}^{(blend)}$ for a binary blend (or $v_{cell}^{(A\text{-}b\text{-}B)}$ for a diblock copolymer system) as functions of the cell volumes $v_{cell}^{(melt)}$ for the pure components and of the composition. Prior theories for polymer melts generally employ three (or more) parameters (P^*, T^*, and ϱ^*) for each pure component and one or two additional interaction parameters for blends, leading to a grand total of seven or eight parameters for binary systems.

B. Free Energy of Polymer Fluids. The lattice cluster theory[11,12] yields the Helmholtz free energy F_{blend} of a binary blend system in the general form

$$\frac{F_{blend}}{N_l k_B T} = \phi_v \ln \phi_v + \sum_{i=1}^{i=2}\frac{\phi_i}{M_i}\ln\frac{2\phi_i}{M_i} - (\ln z - 1)\sum_{i=1}^{i=2}\left(1 - \frac{1}{M_i}\right)\phi_i + \sum_{j=1}^{j^*}\sum_{l=0}^{j} f_{jl}\phi_1^{\,l}\phi_2^{\,j-l} \quad (2.1)$$

The first three terms on the right-hand side of eq 2.1 provide the combinatorial part of F_{blend}, while the last term represents the noncombinatorial portion as a polynomial in the actual volume fractions ϕ_i. A similar expression for the free energy of a melt follows directly from eq 2.1 by droping the summations over i and by replacing the double sum over j and l in eq 2.1 by a single sum. The resulting formula,

$$\frac{F_{melt}}{N_l k_B T} = \phi_v \ln \phi_v + \frac{\phi}{M}\ln\frac{2\phi}{M} - (\ln z - 1)\left(1 - \frac{1}{M}\right)\phi + \sum_{j=1}^{j^*} f_j \phi^j \quad (2.2)$$

applies equally well to pure homopolymer melts and diblock copolymer systems. A series of our papers[9-12,30] describes the method for generating the coefficients f_{jl} and f_j in eqs 2.1 and 2.2 as double expansions in the inverse lattice coordination number $1/z$ and in the dimensionless microscopic van der Waals attractive energies $\{\epsilon_{\alpha\beta}/k_BT\}$. The coefficients in these double expansions depend, in turn, on the monomer structures of the blend components, the site occupancy indices M_i, and on the diblock composition variable $m = M_A^{(b)}/M_{AB} = (N_A^{(b)}s_A)/M_{AB}$ if the system contains diblock copolymers. The variable m is the generalized lattice model analog of the standard diblock composition variable $f = N_A^{(b)}/(N_A^{(b)} + N_B^{(b)})$. When the expression in eq 2.2 is specialized to a pure homopolymer melt, only one interaction energy $\epsilon_{\alpha\alpha}$ appears. The present calculations of the free energy F for binary blends and homopolymer melts retain terms only through orders $1/z^2$ and $(\epsilon_{\alpha\beta}/k_BT)^2$. This approximation fixes[11] the upper limit of j in the summation of eqs 2.1 and 2.2 as $j^* = 6$. The calculations of the free energy for a diblock copolymer melt from eq 2.2 are limited to first order in $\epsilon_{\alpha\beta}/k_BT$, and, consequently, $j^* = 5$ for this case. Equation 2.1 can be extended easily to ternary A/B/A-*b*-B mixtures, and the general rules for computing the three-body coefficients f_{jlm} are very similar[31] to those derived for binary systems (see ref 31 for technical details). The coefficients f_{ij} and f_j of eqs 2.1 and 2.2 are presented[32] explicitly in our previous papers.[11,12,30] In order to enable the interested readers to program the free energy expressions independently, ref 32 explicitly describes where to find these terms.

While experiments at constant volume are described by the Helmholtz free energy F, the Gibbs free energy G,

$$G \equiv F + PV = F + PN_l v_{cell}$$

is designed especially for systems at constant pressure. The pressure P is computed from eq 2.1 as

$$P(T,\phi_v,v_{cell}^{(blend)},\Phi_1) \equiv -\left.\frac{\partial F_{blend}}{\partial V_{blend}}\right|_{T,n_1,n_2} = -\frac{1}{v_{cell}^{(blend)}}\left.\frac{\partial F_{blend}}{\partial n_v}\right|_{T,n_1,n_2} \quad (2.3a)$$

or specializing to a melt as

$$P(T,\phi_v,v_{cell}^{(melt)}) \equiv -\left.\frac{\partial F_{melt}}{\partial V_{melt}}\right|_{T,n} = -\frac{1}{v_{cell}^{(melt)}}\left.\frac{\partial F_{melt}}{\partial n_v}\right|_{T,n} \quad (2.3b)$$

The equations of state derived from eqs 2.3a and 2.3b are used to determine ϕ_v for binary blends and melts, respectively. A pure homopolymer melt has $\Phi_1 \equiv \Phi =$

1, and the pressure computed from the LCT free energy F_{melt} is then a function of only the three parameters T, ϕ_v, and $v_{cell}^{(melt)}$.

C. SANS Interaction Parameter χ_{eff} for Binary Polymer Blends. Small-angle neutron scattering (SANS) experiments for polymer systems provide directly the differential cross section $d\sigma(q)/d\Omega$ per unit volume V. This quantity is also called the absolute scattering intensity $I(q)$. The standard analysis of the SANS data involves the extrapolation of $I(q)$ to zero angle and the use of the incompressible random phase approximation[33] (RPA). This analysis produces the effective Flory interaction parameter χ_{eff}, an important quantity for predicting the thermodynamic properties of polymer systems. The present subsection describes how the scattering intensity $I(0)$ may be computed from the lattice cluster theory and the generalized lattice model.

Neutron scattering theory yields an expression for $I(0)$ in terms of the partial structure factors $S_{ij}(0)$ and the monomer scattering lengths b_i and b_j,[34]

$$I(0) \equiv \frac{1}{V}\frac{d\sigma(0)}{d\Omega} = \frac{1}{V}[n_1N_1 + n_2N_2][b_1^2S_{11}(0) + b_2^2S_{22}(0) + 2b_1b_2S_{12}(0)] \quad (2.4)$$

The term $[n_1N_1 + n_2N_2]$ in eq 2.4 represents the total number of monomers in the system, and the $S_{ij}(0)$ are defined below in eq 2.6 on a per-monomer basis. Replacing the total volume V by $V = N_1v_{cell}^{(blend)}$ converts eq 2.4 into a more convenient form,

$$I(0) \equiv \frac{1}{V}\frac{d\sigma(0)}{d\Omega} = \frac{1-\phi_v}{v_{cell}^{(blend)}}\left[\frac{\Phi_1}{s_1} + \frac{\Phi_2}{s_2}\right][b_1^2S_{11}(0) + b_2^2S_{22}(0) + 2b_1b_2S_{12}(0)] \quad (2.5)$$

where s_i designates the number of lattice sites occupied by a single monomer of species i and where ϕ_v denotes the free volume fraction. Equation 2.5 includes the scattering from both species, for generality, but most cases studied have the scattering dominated by a single component. The zero wave vector partial structure factors $S_{ij}(0)$ of eqs 2.4 and 2.5 are related to the chemical potentials μ_1 and μ_2 by[35]

$$S_{ij}(0) = \frac{N_iN_jk_BT}{n_1N_1 + n_2N_2}\left.\frac{\partial n_j}{\partial \mu_i}\right|_{T,V,\mu_{k\neq i}} \quad (2.6)$$

The chemical potentials μ_1 and μ_2, in turn, are calculated from the free energy (2.1) as

$$\mu_\alpha = \left.\frac{\partial F}{\partial n_\alpha}\right|_{T,V,n_\beta} \quad (2.7)$$

where the volume V in eq 2.7 is evaluated from the equation of state in order to compare with experiments for which the scattering cells are maintained at constant pressure. Hence, the use of the LCT free energy F_{blend} and eqs 2.3 through 2.7 enables us to determine the absolute scattering intensity $I(0)$ from the lattice cluster theory. The effective interaction parameter $\Gamma \equiv \chi_{eff}/v_0$ is now *defined* by the same formula that is used[16,17,21] in the experimental analysis of $I(0)$,

$$\frac{k_N}{I(0)} = \frac{1}{N_1v_1\Phi_1} + \frac{1}{N_2v_2\Phi_2} - 2\Gamma \quad (2.8)$$

where $k_N = N_{Av}[b_1/v_1 - b_2/v_2]^2$ is the scattering contrast factor, N_{Av} is Avogadro's number, and v_1 and v_2 are the molar monomer volumes for pure components 1 and 2, respectively. The calculation of Γ from eq 2.8 is superior to our previously used[12-14] procedure which involves determining χ_{eff} directly from the LCT $S(0)$ and which requires the specification of a normalizing volume v_0. Previously, we adopted[13] the standard approximation $v_0 = (v_1v_2)^{1/2}$, but this choice is arbitrary and is unnecessary now. All experimental data are likewise analyzed with eq 2.8 in order that the experimental and theoretical χ_{eff} refer to identical quantities.

D. Volume of Mixing for a Binary Polymer Blend. The excess volume $V^e \equiv \Delta V = (V_{blend} - V_1 - V_2)$ for a binary blend is the difference between the blend volume V_{blend} and the sum of the volumes V_1 and V_2 for the pure components that are mixed to produce the blend. Our previous computations[13] of the ratio $\Delta V/(V_1 + V_2)$ use the simplifying assumption of identical unit cell volumes for the blend and for both of the pure components. Since section III describes our fitting of the pure melt cell volumes to *PVT* data and since the fitted cell volumes must differ for these components, we lift the assumption of equal volumes. This more general LCT formulation leads to the modified formula

$$\frac{\Delta V}{V_1 + V_2} = \frac{v_{cell}^{(blend)}}{\dfrac{\phi_1}{1-\phi_v^{(1)}}v_{cell}^{(1)} + \dfrac{\phi_2}{1-\phi_v^{(2)}}v_{cell}^{(2)}} - 1 \quad (2.9)$$

where ϕ_1 and ϕ_2 are the actual volume fractions in the blend and $\phi_v^{(i)}$ denotes the free volume fraction in the pure melt of species i. The parameters $v_{cell}^{(1)}$ and $v_{cell}^{(2)}$ are fit to *PVT* data for the pure melts 1 and 2, while the blend unit cell volume $v_{cell}^{(blend)}$ is estimated in terms of $v_{cell}^{(i)}$ and compositions Φ_i by applying the combining rule discussed in section III. The relation in eq 2.9 is generally valid for arbitrary values of the three cell volumes. Taking the simplifying limit of $v_{cell}^{(1)} = v_{cell}^{(2)} = v_{cell}^{(blend)}$ in eq 2.9 recovers our earlier approach.[13] The use of eq 2.9 also illustrates the ability for introducing successive modifications of the lattice model to improve the representation of reality by the LCT.

E. SANS Effective Interaction Parameter χ_{eff} for Diblock Copolymer Melts. Since the absolute scattering intensity $I(0)$ vanishes for an incompressible model description of a diblock copolymer melt, its effective interaction parameter χ_{eff} is generally defined in a different fashion than the χ_{eff} for a binary blend. The traditional incompressible random phase approximation (RPA) analysis of scattering from a copolymer melt represents[36] χ_{eff} in terms of the scattering intensity $I(q^*)$ as

$$\chi_{eff} = \frac{1}{2}\left[\frac{k_N}{I(q^*)} - P(q^*)\right] \quad (2.10)$$

where q^* corresponds to the wave vector for which $I(q)$ is a maximum,

$$\left.\frac{\partial I(q)}{\partial q}\right|_{q=q^*} = 0 \quad (2.11)$$

The definition of the scattering contrast factor k_N remains the same as that for binary blends. The quantity $P(q)$ is given by

$$P(q) = \frac{P_{AA}(q) + P_{BB}(q) + 2P_{AB}(q)}{P_{AA}(q)P_{BB}(q) - [P_{AB}(q)]^2} \quad (2.12)$$

and depends on the radii of gyration R_α (α = A and B) for two blocks, the polymerization indices $N_\alpha^{(b)}$, and the diblock composition variable f through the expressions

$$P_{\alpha\alpha}(q) = fN_\alpha^{(b)}D(q^2R_\alpha{}^2), \quad \alpha = \text{A and B} \quad (2.13a)$$

and

$$P_{AB}(q) = fN_B^{(b)}[1 - {}^1/_2q^2R_A{}^2D(q^2R_A{}^2)][1 - {}^1/_2q^2R_B{}^2D(q^2R_B{}^2)] \quad (2.13b)$$

where $D(q^2R_\alpha{}^2)$ designates the ideal single-chain Debye function,

$$D(q^2R_\alpha) = \frac{2}{q^2R_\alpha{}^2}\left[1 - \frac{1}{q^2R_\alpha{}^2}\{1 - \exp(-q^2R_\alpha{}^2)\}\right] \quad (2.14)$$

The radii of gyration R_α in eqs 2.13 and 2.14 are assumed to be ideal, i.e., proportional to the unperturbed Kuhn lengths l_α,

$$R_\alpha = \left(\frac{1}{6}N_\alpha^{(b)}\right)^{1/2}l_\alpha \quad (2.15)$$

The absolute scattering intensity $I(q^*)$ in eq 2.10 is expressed in terms of the partial structure factors $S_{\alpha\beta}(q^*)$ in an analogous fashion as $I(0)$ is written in terms of $S_{ij}(0)$ for binary blends (see eq 2.4).

Comparisons of LCT computations with experiment, using either compressible or incompressible models, indicate the necessity for treating diblock copolymer melts with a compressible theory. Thus, we require a description of the scattering intensity that incorporates the influence of compressibility. Such a theoretical approach is provided by the compressible RPA theory of Tang and Freed,[37] extended[28] by us to the generalized lattice model of diblock copolymers. This compressible RPA formulation coincides with the PRISM theory[6] expressions for $S_{\alpha\beta}(q)$ if the direct correlation functions $C_{\alpha\beta}(q)$ are taken as constants. The compressible RPA expressions for $S_{\alpha\beta}(q)$ involve three microscopic interaction parameters $\chi_{\alpha\beta}$. The latter, however, cannot be obtained from the individual $S_{\alpha\beta}(0)$ because these $S_{\alpha\beta}(0)$ become linearly dependent[28] for a diblock copolymer system. For cases where the corresponding A/B binary blend would be phase separated, we adopt the approximation of taking the χ_{AA} and χ_{BB} from the LCT computations for the pure homopolymer melts. This choice enables the determination of the remaining interaction parameter χ_{AB} by equating the sum $S_{tot}(0) = S_{AA}(0) + S_{BB}(0) + 2S_{AB}(0)$ from the LCT to that from the compressible RPA. (For more details, see ref 28). This method of calculating χ_{eff} from eq 2.10 again eliminates the necessity of converting the theoretical LCT χ_{eff} on a per lattice site basis to a χ_{eff} on a per monomer basis in order to make adequate comparisons with the experimental χ_{eff}.

III. Computations and Results

Following the general philosophy of theories for fluid mixtures, we begin by determining the single-species parameters through comparison of theory with experiment for the pure components.

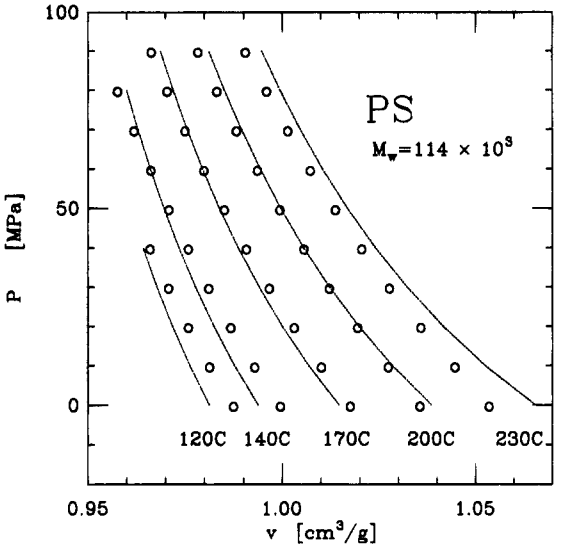

Figure 2. LCT fit to experimental *PVT* data[24] for a pure PS melt. Data presented as a series of isotherms.

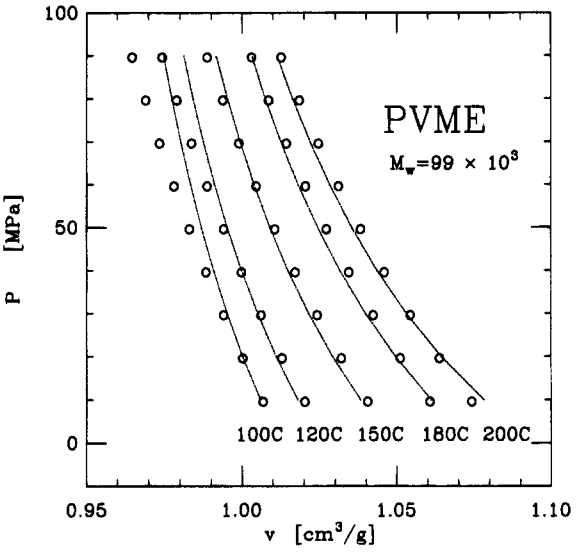

Figure 3. Same as Figure 2 but for a pure PVME melt.

A. *PVT* Properties of Pure PS and PVME Melts. The lattice cluster theory is applied in this subsection to describe the equation of state properties of PS and PVME melts. The theory employs two adjustable parameters: the nearest neighbor van der Waals attractive self-interaction energy ϵ_{i-i} and the volume $v_{cell}^{(i)}$ of a unit cell. These two parameters are determined by fitting eq 2.3b to experimental *PVT* data. The fits are produced by combining an analysis of total least squares deviations between theory and experiment with a visual inspection of the fits. The visual inspection is useful because, as explained below, the mean squares deviations exhibit broad minima.

Figure 2 displays the *PVT* isotherms generated by the LCT for the pure PS melt along with the experimental data of Ougizawa et al.,[24] while Figure 3 depicts the same quantities for the PVME system. The "experimental" isotherms in Figures 2 and 3 are constructed by interpolation of the original isobaric *PVT* data.[24] This interpolation proceeds by least squares fitting the experimental specific volumes v at a given pressure P as a linear function of temperature in the form $v = v'(P) + \alpha(P)T$, thereby allowing us to construct experimental isotherms at arbitrary intermediate T. We, however, exclude data for the region near and below the glass

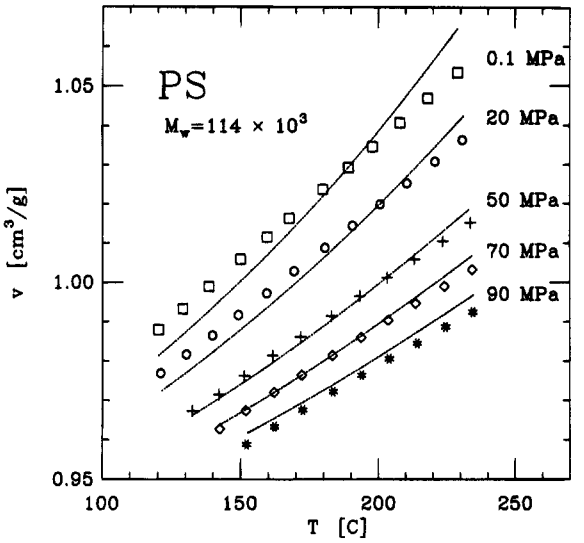

Figure 4. Same as Figure 3 but for a series of isobars.

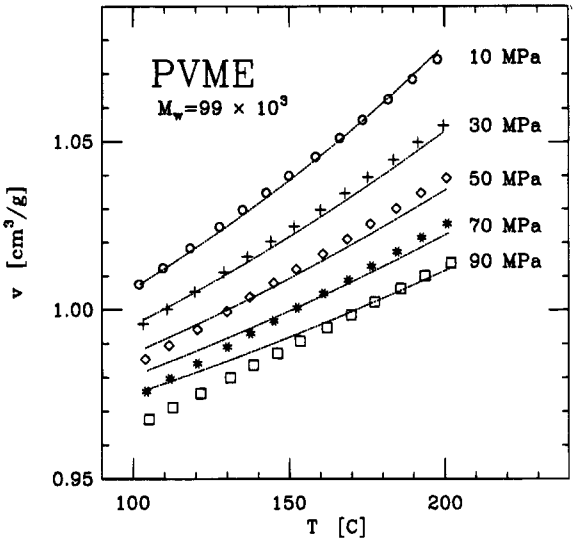

Figure 5. Same as Figure 3 but for a series of isobars.

transition temperature. Rather few data points are available in this glass region for $P = 1$ atm, but the glassy regime grows rapidly with increasing pressure (see Figure 1 of ref 24 for more quantitative details). Both Figures 2 and 3 consider the least squares deviations in fitting the specific volumes. This procedure departs from the commonly used least squares fitting to the pressures, a procedure which overemphasizes the highest pressure regime and even permits the appearance from the fitted theory of negative pressures in the lowest pressure regime. Focusing on the mean squares deviations of the specific volumes, on the other hand, more uniformly weights the data at all pressures and ensures that the theoretical pressures are positive.

The self-interaction energies and the unit cell volumes for the two melts are found to be $\epsilon_{S-S} = 0.620k_BT_0$ and $v_{cell}^{(PS)} = 17.4082$ Å^3 versus $\epsilon_{VME-VME} = 0.590k_BT_0$ and $v_{cell}^{(PVME)} = 22.6004$ Å^3 ($T_0 = 415.15$ K). The fits in Figures 2 and 3 are, however, not totally unique as there exists a 5% range of ϵ_{S-S} between $0.620k_BT_0$ and $0.655k_BT_0$ and of $\epsilon_{VME-VME}$ between $0.565k_BT_0$ and $0.590k_BT_0$ that almost equally well reproduces the experimental data, provided that a slight adjustment is also introduced for $v_{cell}^{(i)}$. The largest discrepancies from experiment appear for PS at low pressures, while the fit for PVME contains deviations mainly in the regime of high pressures and low temperatures. The existence of 1 atm pressure *PVT* data for PS and the absence of experimental data for PVME below about 100 atm do not seem to be responsible for this different behavior. The ranges obtained for the two sets of adjustable parameters are practically unchanged when fits are, alternatively, based on the original experimental *PVT* data and the least squares deviations from specific volumes as is used to generate the *PVT* isobars shown in Figures 4 and 5.

All the fits in Figures 2–5 employ the data for one of the highest available molecular weight samples ($M_w^{(PS)} = 114\,000$ and $M_w^{(PVME)} = 99\,000$) in order to eliminate the dependence of the *PVT* properties (and hence of the adjustable parameters) on molecular weights. Ougizawa et al.[24] exhibit the expected $1/M$ molecular weight dependence of their three pure component adjustable parameters in the range of low molecular weights, but much of this region involves molecular weights that are perhaps too small for descriptions based on completely flexible chain models. Figure 6 provides the *PVT* isotherms of PS as computed from the LCT for the same parameters $\epsilon_{S-S} = 0.62k_BT_0$ and $v_{cell}^{(PS)} = 17.4082$ Å^3 used to produce the isotherms in Figure 2 but for an even higher molecular weight $M_w^{(PS)} = 2100 \times 10^3$ sample. The similar agreement with the experimental data in Figure 6 indicates that the $M_w^{(PS)} = 114 \times 10^3$ sample is also appropriate for representing the high molecular weight behavior of a PS melt. The fits in Figures 2 and 4 use the 114×10^3 molecular weight sample data because it is the only sample for which 1 atm *PVT* data are available.

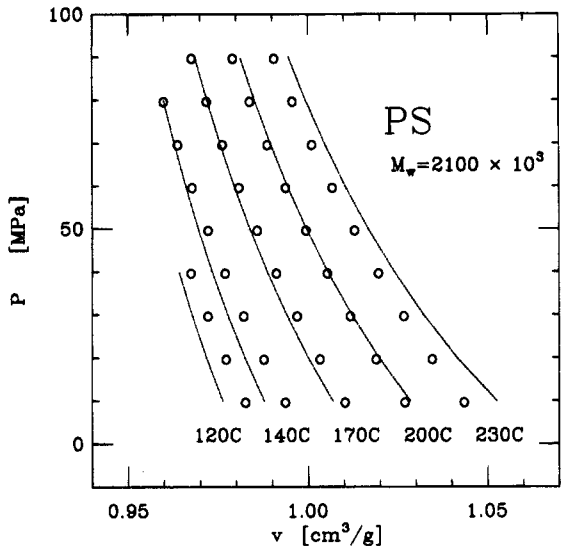

Figure 6. Comparison of LCT predictions with *PVT* data[24] for a $M_w = 2100 \times 10^3$ molecular weight sample of PS.

Generally, the fits in Figures 2–5 are improved somewhat by including a third adjustable parameter. We have produced improved fits (not shown) by adding a parameter that describes a linear variation of $v_{cell}^{(i)}$ (or $a_{cell} = v_{cell}^{1/3}$) with temperature. Alternative choices of a third parameter should improve matters further. However, our two-parameter fits appear adequate for the ultimate purpose of predicting the blend thermodynamics from the properties of the pure components. In addition, the use of two-parameter *PVT* fits controls the proliferation of adjustable parameters and also requires less extensive experimental data for their determina-

tion. Moreover, the LCT fits for low pressures do not appear worse than previous fits[18,19] that use an equation of state involving the three adjustable thermodynamic parameters P^*, V^*, and T^*. As a matter of fact, the strict maintenance of the lattice model would imply that these parameters are not all independent. The separation into three thermodynamic parameters is sensible in a thermodynamic sense, but our desire is to obtain greater microscopic understanding. Thus, we retain the microscopic definitions of the adjustable parameters.

Our fits are restricted to *PVT* data for moderate pressures, say $P < 100$ MPa, partially because we use only two adjustable parameters, but other approaches with three parameters also find that the fitted parameters vary with temperature and pressure range considered.[20] However, this restriction is also influenced by the knowledge of the inadequacy of the term $\phi_v \ln \phi_v$ (see eq 2.2) for describing the entropy associated with the distribution of free volume. This entropic contribution should require some modifications, especially at high pressures. However, any attempt in this direction, such as that provided by using the Flory equation of state form, must lead to a further proliferation of adjustable parameters which we prefer to avoid as long as possible. Fits (not shown) to higher pressure *PVT* data between 100 and 200 MPa actually display even better agreement with experiment than that in Figure 2 or 3. The two adjustable parameters, the cell volume $v_{cell}^{(PS)}$ and van der Waals energy ϵ_{S-S}, for the higher pressure data are, respectively about 2 and 5% lower than the values obtained from the fit in Figure 2, and this small variation is almost within the general range of uncertainty in the fits of the parameters. We focus on describing the lowest pressure data because the majority of the available scattering data for the binary polymer blends are for a pressure of 1 atm and because the recent higher pressure data[16,17] also falls almost entirely in the range considered in Figures 2–5.

B. SANS Properties of PS/PVME Blends at P = 1 atm. When applied to binary polymer systems, the LCT involves four adjustable parameters: three van der Waals interaction energies $\epsilon_{\alpha\beta}$ and the volume $v_{cell}^{(blend)}$ of the unit cell. Subsection A shows that the cell volumes differ for individual pure components and must therefore also differ for the blend. The blend unit cell is determined from the known pure melt volumes $v_{cell}^{(PS)}$ and $v_{cell}^{(PVME)}$ from subsection A by applying the common combining rule,[38]

$$v_{cell}^{(blend)} = v_{cell}^{(PS)}\Phi_1^{\,2} + v_{cell}^{(PVME)}\Phi_2^{\,2} + 2\left[\frac{(v_{cell}^{(PS)})^{1/3} + (v_{cell}^{(PVME)})^{1/3}}{2}\right]^3 \Phi_1\Phi_2 \quad (3.1)$$

On the other hand, the use of the standard geometric mean combining rule[39] for the heterocontact van der Waals interaction energy ϵ_{S-VME},

$$\epsilon_{S-VME} = (\epsilon_{S-S}\epsilon_{VME-VME})^{1/2} \quad (3.2)$$

leads, as shown below, to gross errors in predicting the phase diagram and other thermodynamic and scattering properties of the PS/PVME blends. Our LCT calculations exhibit the extreme sensitivity of these blend quantities to ϵ_{S-VME}. Thus, determining ϵ_{S-VME} from experimental data is the only method for obtaining a useful value of ϵ_{S-VME}. Since *PVT* data are not available for PS/PVME blends, the single adjustable parameter ϵ_{S-VME} is fit to the SANS scattering data of Han et al.[23] Their extensive data cover a wide range of compositions, temperatures, and molecular weights, thereby providing a very stringent test of the single energy parameter LCT for blends. The two other energy parameters ϵ_{S-S} and $\epsilon_{VME-VME}$ are taken from our fits to pure melt *PVT* data as described in subsection A. The tiny (<1%) differences between self-interaction energies ϵ_{S-S} in hydrogenated and perdeuterated polystyrene are much smaller than the spreads of acceptable values for ϵ_{S-S} and $\epsilon_{VME-VME}$ that are obtained from the fits to pure melt *PVT* data. (Subsection E provides an illustration of these small isotopic differences.) Thus, these differences may be ignored as minor corrections for the PS/PVME blends, but not of course, for PSD/PSH blends where the ϵ_{S-S} isotopic differences represent almost everything.

Figures 7a–c compare the SANS data of Han et al.[23] for the effective interaction parameter χ_{eff} with the LCT computations. Both the experimental analysis and the LCT computations use eq 2.8 to define χ_{eff} in terms of the absolute scattering intensity. These figures exhibit χ_{eff} as a function of composition over a wide range of temperatures for three different molecular weight samples of PS/PVME. The energy parameter ϵ_{S-VME} is found to be $\epsilon_{S-VME} = 0.607675 k_B T_0$. (The extra significant digits come from optimizing the fits and from the sensitivities mentioned above.) This ϵ_{S-VME} departs from the geometrical mean $(\epsilon_{S-S}\epsilon_{VME-VME})^{1/2} = 0.604814\ k_B T_0$ by less than 0.5%. However, this small difference is sufficient to change the phase diagram completely from a LCST (lower critical solution temperature) phase diagram, observed experimentally and predicted for the fitted ϵ_{S-VME}, to a calculated UCST (upper critical solution temperature) phase diagram for the geometrical mean ϵ_{S-VME}. This example graphically illustrates the futility of using simple combining rules like eq 3.2 for the heterocontact interactions, and it also suggests caution in attempting to compute ϵ_{S-VME} from molecular mechanics or other "theories".

The agreement between LCT computations and experiment in Figures 7a–c is quite good. The effective interaction parameter χ_{eff} depends only weakly on the molecular weights of both components because the molecular weights in all three samples are sufficiently high. A small sensitivity of χ_{eff} to molecular weights follows from the theoretical prediction of the presence of $1/M_i$-dependent corrections which are negligible for large M_i. The experimental data also concur with the absence of a molecular weight dependence, but this is partially obscured by the presence of much larger experimental errors for the lowest molecular weight sample (see Figure 7c).

Figures 7a–c display the "experimental" data in the form of χ_{eff}/v_0 as presented by Han et al.[23] and many others. An alternative is to present the directly measured extrapolated zero-angle scattering intensities $I(0)$. However, the $I(0)$ cover a wider range of values, making the presentation of the data in the form of χ_{eff}/v_0 much more transparent. In fact, the $I(0)$ curves for different temperatures overlap or even blur into each other at higher compositions, whereas the curves for χ_{eff}/v_0 are more separated. A proper comparison between theory and experiment in Figures 7a–c requires that the computed theoretical intensities $I(0)$ are analyzed using the same formula for χ_{eff}/v_0 (see eq 2.8) as is applied in the analysis of the experimental differential cross section data. Our previous procedure[12–14] computes χ_{eff}

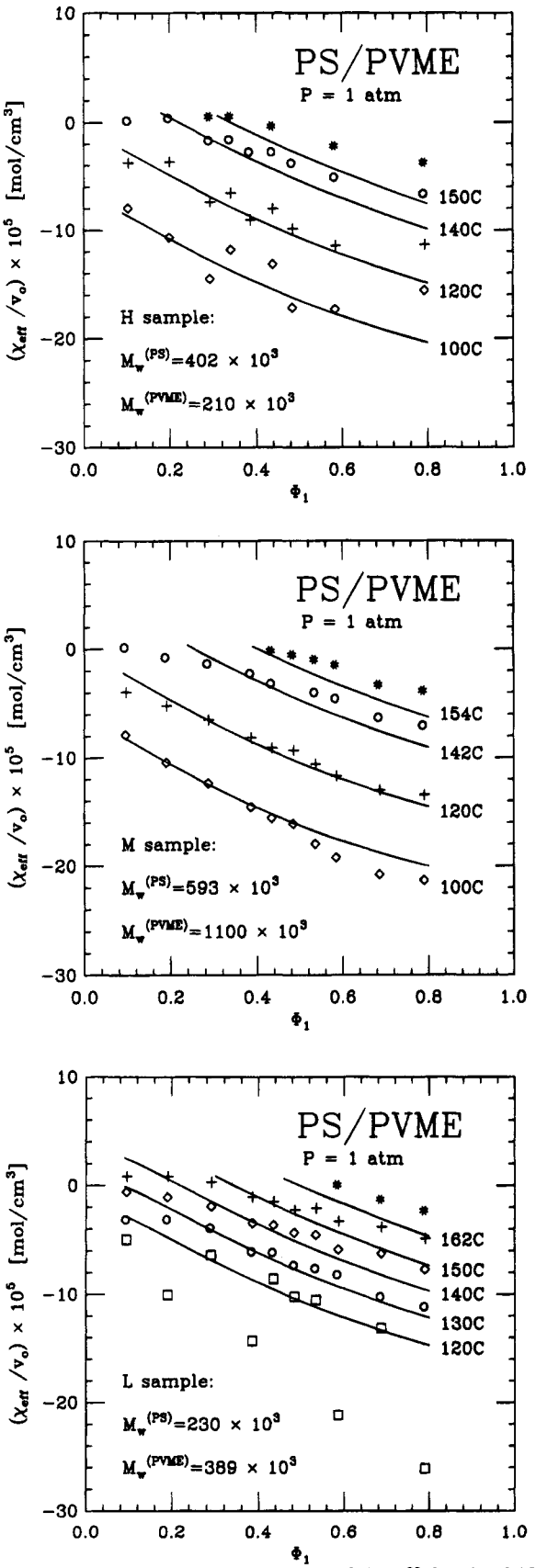

Figure 7. LCT fit to the experimental data[23] for the SANS effective interaction parameter χ_{eff}/v_0 for three different PS/PVME blend samples: (a) H sample; (b) M sample; (c) L sample. Both the experimental analysis and the LCT computations use eq 2.8 to define χ_{eff}/v_0 in terms of the absolute scattering intensity $I(0)$.

on a per lattice site basis from the LCT and then converts this to the form of χ_{eff}/v_0 per monomer as is used for the experimental data. The present method is superior in requiring no assumption concerning the normalizing volume v_0 or the scattering contrast.

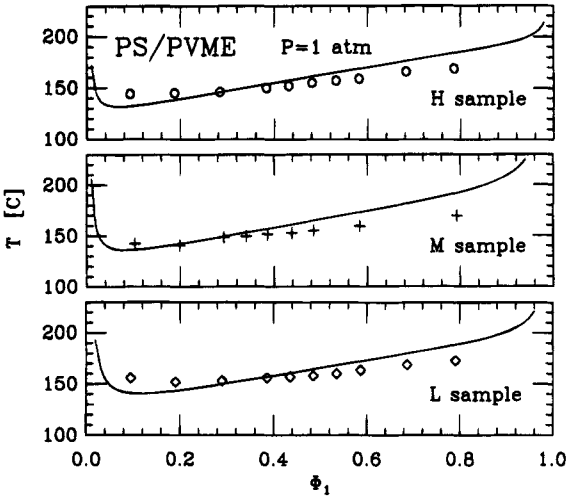

Figure 8. Comparison of the LCT predictions with the experimental data of Han et al.[23] for the spinodal curves [defined from the vanishing of $1/I(0)$] of the three PS/PVME blend samples.

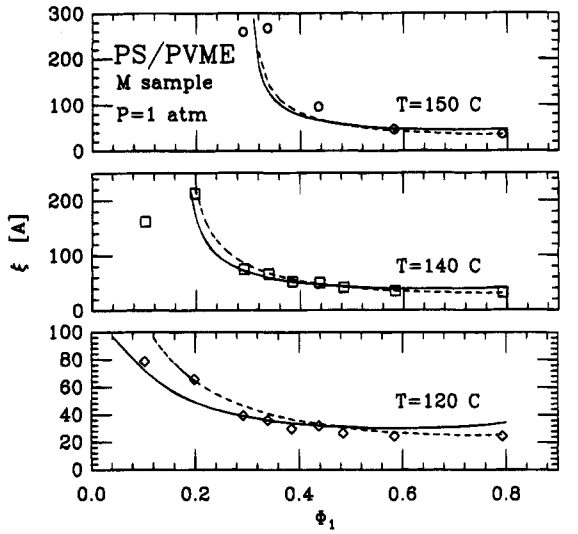

Figure 9. Comparison of the LCT predictions with the SANS experimental data of Han et al.[23] for the composition dependence of the correlation length ξ at various temperatures for the M sample PS/PVME blends. Figure 7 gives the molecular weights.

After determination of ϵ_{S-VME} from the fits in Figures 7a–c, no additional adjustable parameters enter into the further calculations for PS/PVME blends. The computed phase diagrams are compared in Figure 8 with the experimental spinodal data of Han et al.[23] for the three PS/PVME samples. The phase diagrams are presented in the form of spinodals as defined by the vanishing of the inverse scattering intensity $1/I(0)$. The agreement, as in Figures 7a–c, is quite satisfactory but degrades slightly for low and high compositions.

Another comparison between theory and experiment is provided for the correlation length $\xi(\Phi_1)$, defined by

$$I(q) = \frac{I(0)}{1 + q^2\xi^2}, \qquad q \to 0$$

Figure 9 compares LCT computations with experiment for $\xi(\Phi_1)$ as a function of blend composition at different temperatures for the M sample PS/PVME blend.

The composition variation of $\xi(\Phi_1)$ and the quality of the fit to the experimental data for the remaining two PS/PVME samples are rather similar to those illustrated in Figure 9. The computations employ the compressible random phase approximation in the manner described in ref 40. The solid and dashed lines in Figure 9 correspond, respectively, to using unperturbed ($l_{PS,0}$ and $l_{PVME,0}$) and perturbed (i.e., composition dependent) Kuhn lengths l_{PS} and l_{PVME}. The latter are obtained from ad hoc one-parameter fits of the form[41] (not valid for Φ_S near 0 or 1),

$$l_{PS} = l_{PS,0} \exp[A(1 - \Phi_{PS})] \quad (3.3a)$$

$$l_{PVME} = l_{PVME,0} \exp[-B(1 - \Phi_{PVME})] \quad (3.3b)$$

to experimental data[23] for the effective radius of gyration. The superiority of employing the perturbed lengths in Figure 9 is perhaps debatable. Using perturbed lengths introduces a small improvement at higher compositions, but this occurs at the expense of worsening the reproduction of experimental data for ξ at low compositions. The perturbed lengths are only really required to rationalize the experimental data[23] (not shown) for the composition dependence of the apparent radius of gyration.

C. Volume of Mixing for PS/PVME Blends at P = 1 atm. The incompressibility assumption has been central to many theories of polymer fluids and still persists, for instance, in the usual analysis of SANS data. On the other hand, polymer blends are compressible fluids, exhibiting a nontrivial equation of state. Several experiments provide data that cannot be explained without lifting this conventional incompressibility assumption. The simplest example is posed by the volume change on mixing ΔV, a pure thermodynamic quantity which vanishes identically for an incompressible model. Measurements for a PS/PVME blend show[42] that ΔV is the order of 0.3% at room temperature and P = 1 atm. The question of whether the LCT with no further adjustable parameters is capable of reproducing this small ΔV provides one stringent test for the LCT blend theory.

Figure 10 compares LCT computations for PS/PVME blends with the experimental data of Shiomi et al.[42] The agreement between theory and experiment is quite good. The dashed curve in Figure 10 describes the LCT prediction generated by using eq 3.1 with the cell volumes $v_{cell}^{(PS)}$ and $v_{cell}^{(PVME)}$ that are determined from the fits to the pure melt PVT data as described in subsection A. Since the ΔV measurements are available for an experimental temperature T = 50 °C which lies much below the lowest temperatures considered in the fits of Figures 2–5 (100 °C for PVME and 120 °C for PS) and also below the PS glass transition temperature $T_g^{(PS)}$ = 373 K, it is dubious as to whether the above $v_{cell}^{(PS)}$ and $v_{cell}^{(PVME)}$ values apply for T = 50 °C. Hence, the solid curve in Figure 10 displays the LCT computations for $\Delta V/(V_1 + V_2)$ at T = 50 °C when the pure component $v_{cell}^{(PS)}$ and $v_{cell}^{(PVME)}$ are taken from lower temperature experimental data.[24] This modification of cell volumes indeed improves the agreement of theory with experiment. The corrected unit cell volumes at T = 50 °C and P = 1 atm are determined from the equations of state (2.3b) and from the lattice model relation between $v_{cell}^{(i)}$ and specific volume v at given temperature T and pressure P,

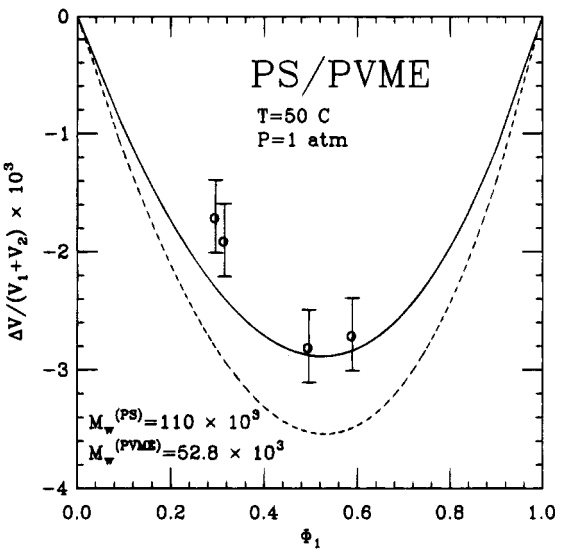

Figure 10. Comparison of the LCT prediction for fractional excess volume of PS/PVME blends against the experimental data of Shiomi et al.[42] The solid curve represents the LCT calculation when the volume $v_{cell}^{(PS)}$ is estimated from the lower temperature PVT data,[24] while the dashed curve corresponds to using the high-temperature $v_{cell}^{(PS)}$ determined from the LCT fits in Figures 2 and 4.

$$v_{cell}^{(i)} = \frac{v[1 - \phi_v^{(i)}]M_{mon}^{(i)}}{N_{Av}s_i} \quad (3.4)$$

where $\phi_v^{(i)}$ designates free volume fraction in the pure melt of species i, $M_{mon}^{(i)}$ denotes its monomer molecular weight, s_i is the number of lattice sites occupied by a single monomer of species i, and N_{Av} is Avogadro's number. Equation 3.4 is substituted into the equation of state, and the quantity $\phi_v^{(i)}$ is determined by an iterative procedure. The convergence is usually achieved after less than 100 iterations, and the resultant $\phi_v^{(i)}$ are resubstituted into eq 3.4 along with the experimental T = 50 °C, P = 1 atm specific volume v to compute the "corrected" $v_{cell}^{(i)}$. The "corrected" cell volumes $v_{cell}^{(i)\prime}$ at T = 50 °C and P = 1 atm are slightly different than those determined from Figures 2–5, $v_{cell}^{(PS)\prime}$ = 17.7252 Å^3 vs $v_{cell}^{(PS)}$ = 17.4082 Å^3 and $v_{cell}^{(PVME)\prime}$ = 22.3389 Å^3 vs $v_{cell}^{(PVME)}$ = 22.6004 Å^3. Because PVT data are not available for PVME at P = 1 atm, the specific volumes for a PVME melt are taken for the lowest experimental pressure, which is about 100 atm. It is not surprising that ΔV at 1 atm is much more sensitive to the choice of the cell volumes $v_{cell}^{(i)}$ and to the form of combining rule for $v_{cell}^{(blend)}$ than is the P = 1 atm scattering intensity $I(0)$.

D. Pressure Dependence of the SANS Effective Interaction Parameter χ_{eff} for PS/PVME Blends. The variation of the effective interaction parameter χ_{eff} with pressure is another blend property that cannot be explained by a theory based on an incompressible model because such a model has the pressure undefined. Compressible models, on the other hand, include the presence of excess free volume and lead to a nontrivial equation of state.[43] Our previous LCT computations[12] for binary blends predict the existence in blends of strong pressure variations for the effective interaction parameter χ_{eff}, predictions that have been verified by subsequent experimental studies.[16,17] This subsection compares the pressure-dependent SANS experimental data with LCT calculations based on the parameters determined in the subsections A and B.

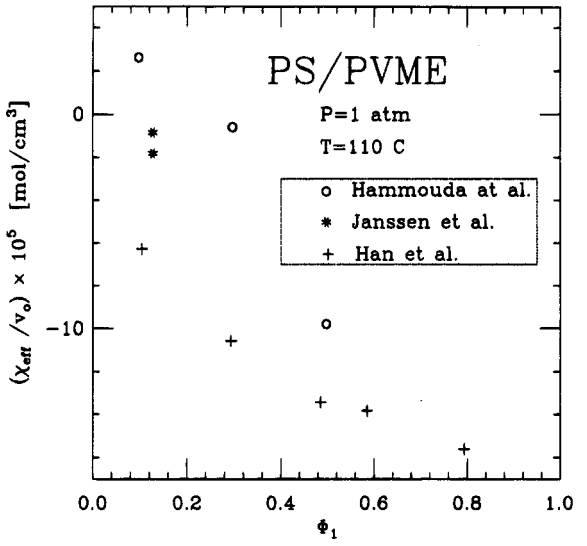

Figure 11. Comparison of experimental data from different groups for the composition dependence of the SANS effective interaction parameter χ_{eff}/v_0 of PS/PVME blends at 1 atm pressure. The original data of ref 16 have been reanalyzed by us in producing this figure and Figures 16–18.

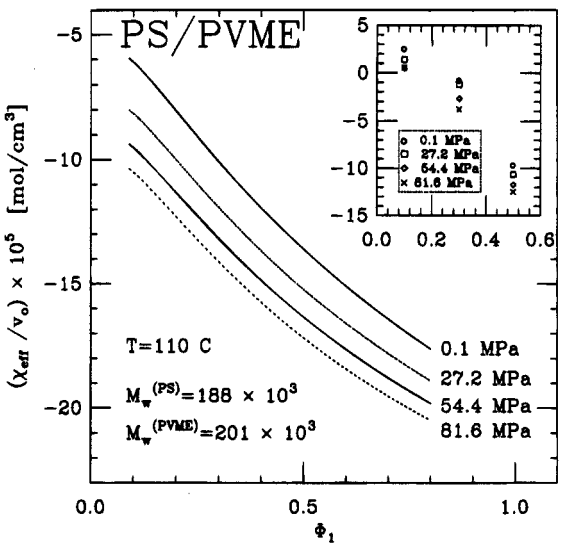

Figure 12. LCT prediction for the variation with composition and pressure of the SANS effective interaction parameter χ_{eff}/v_0 for PS/PVME blends. The inset presents the SANS experimental of Hammouda and Bauer.[17]

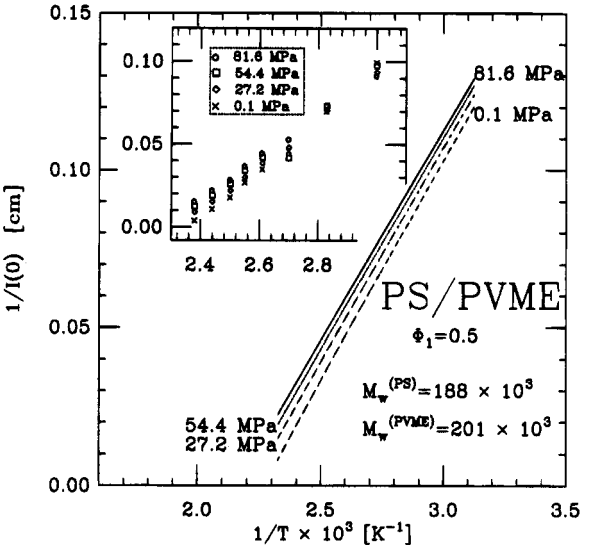

Figure 13. LCT prediction for the temperature and pressure dependence of the inverse absolute scattering intensity $1/I(0)$ for PS/PVME blends. The inset presents the SANS experimental data of Hammouda and Bauer.[17]

The higher pressure SANS data for PS/PVME blends are rather limited compared to the large quantity of 1 atm scattering data of Han et al.[23] This paucity of higher pressure data emerges from experimental difficulties that are associated with the maintenance and the accurate control of high pressures in a small scattering cell. The recent measurements of Hammouda and Bauer[17] consider several pressures and temperatures but only three compositions, while the experiments of Janssen et al.[16] are performed only for a single critical composition ($\Phi_1 = 0.13$) of PS/PVME but cover a wider range of pressures. The 1 atm pressure SANS data from these two groups display some systematic deviations both between each other and from the more extensive data of Han et al.[23] (see Figure 11) when all sets of data are analyzed in a common fashion based on eq 2.8. The constant-pressure cell data are shifted to higher χ_{eff} from the data of Han et al.[23], with the Hammouda–Bauer data[17] shifted somewhat more. The samples used in all three sets of experiments have different molecular weights (indicated in the figures below), but the molecular weights of all samples are high enough to make their differences not be responsible for the inconsistencies shown in Figure 11. (Similar deviations appear for other temperatures.) Several possible reasons exist for these discrepancies, such as different sample preparations, different PVME polydispersities, or different experimental procedures [the use of a constant-volume scattering cell which is held approximately in a $P = 1$ atm environment (Han et al.) versus a constant-pressure scattering cell (Hammouda and Bauer and Janssen et al.)]. We cannot explain the origins of these deviations which, however, present no serious impediments to comparisons with the LCT as we discuss below.

Since the LCT computations with our adjustable parameters provide reasonably good agreement with the SANS data of Han et al.[23] for PS/PVME, the differences in $P = 1$ atm data from the different groups render it impossible to obtain a simultaneous quantitative description for the experimental results of Janssen et al.[16] or of Hammouda and Bauer.[17] Thus, instead of trying to devise another set of $\{\epsilon_{\alpha\beta}\}$ and $\{v_{cell}^{(i)}\}$ that would ensure quantitative agreement with each of these two sets of pressure-dependent SANS experiments, we focus on predicting the general trends that are common to all the data. The LCT computations use the van der Waals interaction energies and the pure melt cell volumes from subsections A and B in conjunction with the combining rule of eq 3.1. Apart from the overall shifts in the χ_{eff} data as exhibited in Figure 11, the LCT predictions described below display similar trends with pressure to those observed by Hammouda and Bauer and by Janssen et al.

Figure 12 displays the computed pressure and composition dependence of the interaction parameter χ_{eff} over a wide range of PS/PVME compositions for $T = 110$ °C, while Figure 13 depicts the pressure and temperature variation of the computed LCT inverse absolute scattering intensity $1/I(0)$ for a single composition $\Phi_1 = 0.5$. The LCT calculations remain in qualitative accord with the experimental data of Hammouda and Bauer, which are shown in the insets to Figures 12 and 13. Generally, at a fixed temperature and blend composition, both the computed and observed χ_{eff} decrease

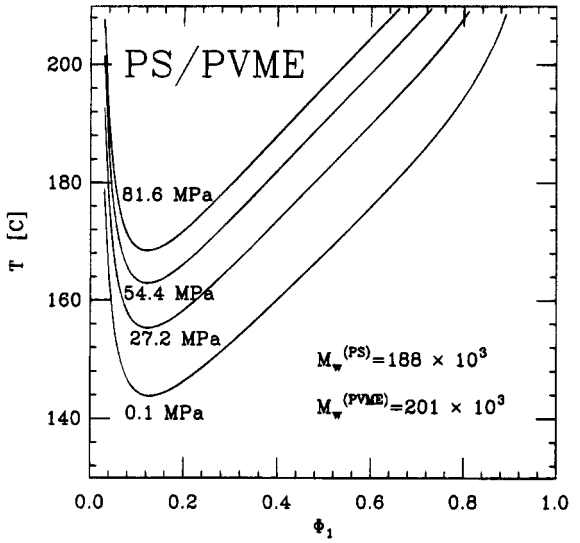

Figure 14. LCT predictions of the spinodal curves [defined from the vanishing of $1/I(0)$] for PS/PVME blends at different pressures.

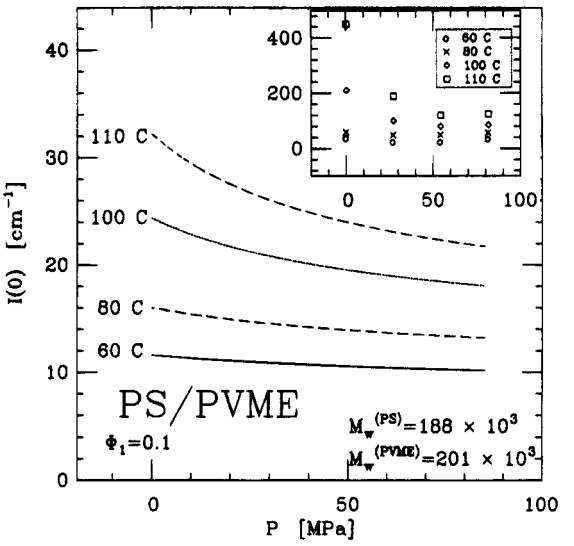

Figure 15. LCT prediction for the pressure dependence of the absolute scattering intensity $I(0)$ for PS/PVME blends at various temperatures. The inset presents the SANS experimental data of Hammouda and Bauer.[17]

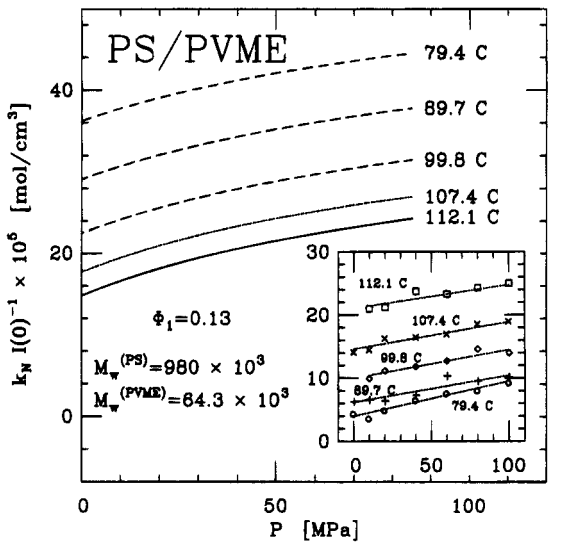

Figure 16. LCT prediction for the pressure dependence of the inverse scattering function $1/S(0) \equiv k_N/I(0)$ for PS/PVME blends at various temperatures. The inset displays the SANS experimental data of Janssen et al., [16] and the straight lines in the insets are least squares fits.

with pressure, while $1/I(0)$ increases. The experimental data of Hammouda and Bauer for a symmetric $\Phi_1 = 0.5$ PS/PVME blend seem to exhibit (see the inset to Figure 13) a reverse trend (not present in the LCT computations) for $1/I(0)$ at lower temperatures.

A more negative χ_{eff} for higher pressures indicates better miscibility for the PS/PVME blend, which in turn implies a shift of the critical temperature and the phase diagram to higher temperatures. This tendency is illustrated in Figure 14 by the LCT computations of the spinodal curves for the same pressures and molecular weights as used in the Hammouda–Bauer experiment. As the pressure increases, the fraction of excess free volume ϕ_v diminishes. Thus, the presence of excess free volume *disfavors* the compatibility of PS/PVME blends and presumably of all blends exhibiting lower critical solution temperatures. This feature of the LCT computations is consistent with the known observation that only a theory that includes blend compressibility can predict LCST behavior (unless the theory is endowed with ad hoc empirical assumptions concerning a composition-dependent χ_{eff}).

The absolute scattering intensity becomes less sensitive to pressure at lower temperatures and higher pressures. This feature is displayed by the LCT calculations, as presented in Figure 15, and by the experimental data of Hammouda and Bauer[17] (see the inset to Figure 15). The general trends for $I(0)$ in Figure 15 do not translate into a similar trend for the $1/I(0)$ (or χ_{eff}). The following simplified example illustrates the origin of these different behaviors for $I(0)$ and $1/I(0)$. If, for simplicity, the absolute scattering intensity $I(0)$ at a given temperature varies linearly with pressure, then $\Delta I(0)/\Delta P = \alpha_P$ yields a constant α_P, whereas $\Delta[1/I(0)]/\Delta P = -\alpha_P/I(0)$ produces a pressure-dependent slope. The growth of the inverse scattering intensity with pressure and temperature also appears in the experimental data of Janssen et al.,[16] which are summarized together with our LCT computations in Figure 16. The straight lines in the inset to this figure provide the least squares fits to the experimental data. The theoretical predictions in Figure 16 are displaced from the experimental data by an almost constant shift.

The conventional analysis of SANS experimental data for χ_{eff}/v_0 at any pressure P involves the separation of the temperature-independent portion Γ_σ of χ_{eff}, called the "entropic" part, from the temperature-dependent contribution, called the "enthalpic" part, following the well-known empirical relation

$$\chi_{eff}/v_0 \equiv \Gamma = \Gamma_\sigma + \Gamma_h \frac{1}{T} \tag{3.5}$$

Hammouda and Bauer note[17] an apparent difference between their measured pressure dependence of both Γ_σ and Γ_h and those obtained by Janssen et al.[16] Our LCT calculations depicted in Figures 17 and 18 display both Γ_σ and Γ_h as varying with pressure, in general agreement with the findings of Hammouda and Bauer.[17] The LCT Γ_σ calculated in Figure 17 for $\Phi_1 = 0.13$ diminishes by about 10% when the pressure changes between 1 and 800 atm, while the LCT Γ_h (see Figure 18) increases by about 5% over the same range of pressures and for the same composition $\Phi_1 = 0.13$. On the other hand, Janssen et al.[16] claim that only the

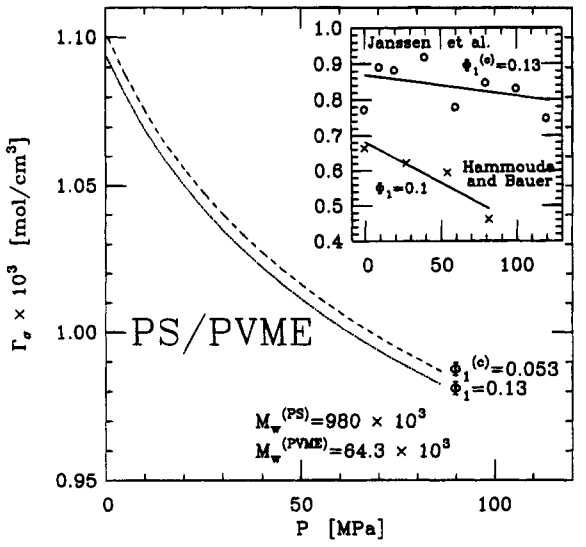

Figure 17. LCT prediction for the pressure dependence of the entropic portion Γ_σ of the effect interaction parameter $\Gamma \equiv \chi_{eff}/v_0$ for PS/PVME blends. The inset presents the Γ_σ that is extracted from the SANS experimental data of Janssen et al.[16] and of Hammouda and Bauer[17] by using an identical analysis as in the theoretical calculations.

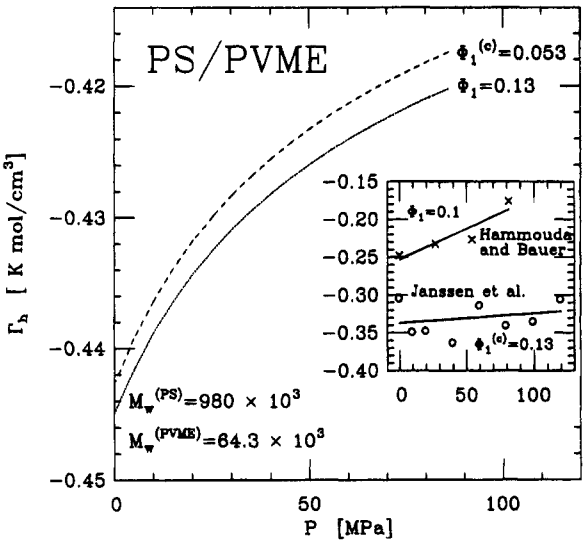

Figure 18. Same as Figure 17 but for the enthalpic portion Γ_h of the effective interaction parameter Γ. Qualitative agreement between theory and experiment (see the inset) is obtained only when the same definition of χ_{eff}/v_0 is employed, as described in the text.

entropic part Γ_σ depends on pressure, while the enthalpic contribution Γ_h is pressure independent. Their data analysis departs, however, from that based on eqs 2.8 and 3.5. Our reanalysis of their original data for $1/S(0) \equiv k_N/I(0)$ uses these two equations for consistency in comparison with the Hammouda–Bauer data and the LCT computations. We fit the interaction parameter Γ (evaluated for a given P from the experimental $1/S(0)$) as a linear function of $1/T$ and then plot the slopes versus pressure. The insets to both Figures 17 and 18 illustrate the results generated by this method, along with experimental data of Hammouda and Bauer. The large spread in both Γ_σ and Γ_h in these insets stems from the large experimental errors in the measurement of the absolute intensities $I(0)$ (see Figure 1 of ref 16). The straight lines in the insets present the least squares fits merely as a guide for the eye in order to compare the reanalyzed Γ_σ and Γ_h with the LCT computations. The overall trends in the pressure dependence of both Γ_σ and Γ_h for the Janssen et al.[16] data are now in accord with those found by Hammouda and Bauer[17] and those emerging from our LCT calculations. The two sets of experimental slopes for Γ_σ differ between each other as do those for Γ_h, and these discrepancies seem to be consistent with those accentuated in Figure 11. We again emphasize that the LCT computations involve no additional adjustable parameters beyond those already fit in subsections A and B.

E. SANS Effective Interaction Parameter χ_{eff} for PB-*b*-PMMA Diblock Copolymer Melt at $P = 1$ atm. By analogy to binary homopolymer blends, the minimal LCT description of diblock copolymer melts requires four adjustable parameters: three van der Waals attractive energies $\epsilon_{\alpha\beta}$ and one volume for the unit cell of the diblock system. An ideal testing ground for the LCT theory of diblock copolymers would be to compare its predictions againt experiment for a PS-*b*-PVME melt, since this comparison would require no new adjustable parameters. The only modification in the procedure would involve altering the combining rule of eq 3.1 by replacing the blend composition Φ_1 by the composition variable f that characterizes the fraction of monomers of type 1 in a single diblock chain (or in the system). The availability of a PS-*b*-PVME melt would permit probing the influence upon the diblock effective interaction χ_{eff} of the junctions between the two blocks. The presence of these junctions distinguishes diblock copolymers from the corresponding homopolymer blends and is responsible for certain differences in thermodynamic behavior of these two chemically related polymer fluids.[27,28,30]

Unfortunately, the PS-*b*-PVME diblock copolymer has not yet been synthesized. Therefore, in order to provide the next best comparison of the diblock copolymer LCT with available SANS experimental data, we choose the PS-*b*-PMMA system which has one chemical species in common with PS/PVME blends. Our above analysis of the *PVT* data for the pure PS melt has already determined ϵ_{S-S}, and $v_{cell}^{(PS)}$, so these parameters are fixed at their values generated by the fits in figures 2 and 4. The absence of pure PMMA melt *PVT* data for pressures of less than about 1000 atm restrains us from using a similar analysis for extracting from the *PVT* data values of $\epsilon_{MMA-MMA}$ and $v_{cell}^{(PMMA)}$ that are appropriate for reproducing the 1 atm SANS data. Thus, both the remaining energies $\epsilon_{MMA-MMA}$ and ϵ_{S-MMA} are fit to the SANS data of Russell et al.[25] for the diblock copolymers. The PMMA cell volume $v_{cell}^{(PMMA)}$ is evaluated from eq 3.4 and the equation of state (2.3b) by applying the common empirical relation

$$v = v_{T_g}[1 + \alpha(T - T_g)] \tag{3.6}$$

with experimental data for the specific volume $v_{T_g} = 0.8696$ cm³/g at the glass transition temperature $T_g = 378$ K and the coefficient of thermal expansion $\alpha = 5.80 \times 10^{-4}$ K^{-1} taken from the literature.[44]

Figure 19 illustrates the fit of the LCT to the temperature dependence of χ_{eff} for two different molecular weight PS-*b*-PMMA samples. The upper line corresponds to scattering mostly from the deuterated PS monomers in PSD-*b*-PMMA, and the adjustable parameters are found to be $\epsilon_{MMA-MMA} = 0.593 k_B T_0$ and $\epsilon_{S-MMA} = 0.6051208 k_B T_0$ with $T_0 = 415.15$ K. The cell volume for the PS-*b*-PMMA diblock melt is evaluated from the combining rule of eq 3.1 with Φ_1 replaced by f and Φ_2

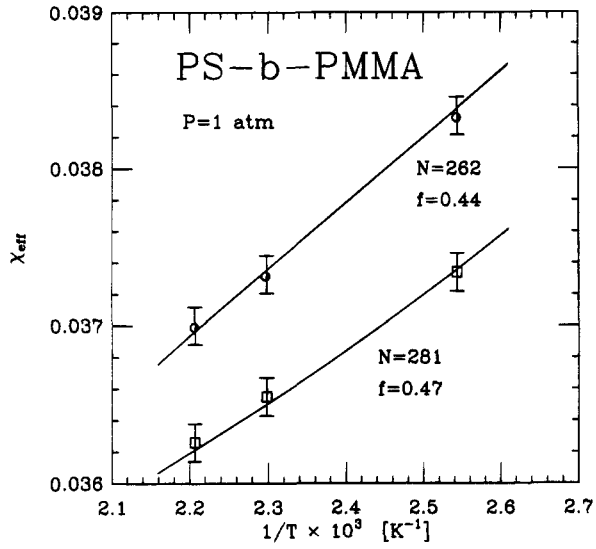

Figure 19. Comparison of LCT calculations for the temperature dependence of the SANS χ_{eff} for PS-*b*-PMMA diblock copolymer melts with the experimental data of Russel et al.[25,26] The upper line corresponds to scattering mostly from deuteriated PS monomers, while the lower one illustrates the case where scattering occurs primarily from deuteriated PMMA monomers.

by $1 - f$. The unit cell volume $v_{cell}^{(PMMA)}$ used in eq 3.1 is determined from eqs 3.4 and 3.6 at the average temperature for the SANS experimental data of Russell et al.,[25] i.e., at $T = 150$ °C, where $v_{cell}^{(PMMA)}$ equals 19.0577 Å^3. This use of a temperature-averaged $v_{cell}^{(PMMA)}$ leads to a slight modification of the heterocontact energy ϵ_{S-MMA} but does not affect the quality of the fit. The lower line in Figure 19 depicts the same dependence of χ_{eff} for a PS-*b*-PDMMA sample, where the scattering occurs mostly from the deuteriated PMMA monomers. Therefore, the fit employs the slightly different $\epsilon_{S-S'} = 0.622k_BT_0$, $\epsilon_{MMAD-MMAD} = 0.591k_BT_0$, and $\epsilon_{S-MMAD} = 605051k_BT_0$. The fitted $\{\epsilon_{\alpha\alpha}\}$ for the fully protonated monomers are very slightly larger than those for the perdeuteriated monomers as expected, with the difference well within a reasonable range. Both fits in Figure 19 describe the experimental χ_{eff} quite well, and the agreement between theory and experiment is even better than the experimental accuracy as represented by the error bars. Likewise, the reproduction of the experimental $I(q)$ curves (not shown) is quite satisfactory.

Our previous LCT computations predict a pressure dependence to the microphase separation transition but not an uncertainty as to whether the $\{\epsilon_{\alpha\beta}\}$ should be permitted to vary with pressure. The analysis in subsection A indicates that the use of pressure-independent $\{\epsilon_{\alpha\beta}\}$ is suitable over moderate pressure ranges. While the new parameter set of $\{\epsilon_{\alpha\beta}\}$ differs a bit from the values previously used, the same general trends would emerge from employing the new parameters.

IV. Discussion

In passing from the Flory−Huggins (FH) lattice model for incompressible polymer blends to a compressible lattice model, the minimum required number of independent microscopic interaction energies grows from one in FH theory to three in the more general lattice cluster theory (LCT). This greater number of interaction energy parameters in the LCT provides a stimulus for investigating optimal methods of determining the parameters from a minimum of experimental data. The procedure used here for the LCT follows the traditional theoretical treatment of fluid mixtures in which the properties of multicomponent systems are represented in terms of the microscopic parameters for the pure components. Particular applications are provided for the widely studied PS/PVME polymer blends. The application of this fluid mixture philosophy is provoked, on the other hand, by the recent availability of experiments probing of the pressure dependence of small-angle neutron scattering (SANS) data for this system, a pressure dependence previously predicted[12] by us on the basis of LCT computations. Another stimulus for the present extensions of the LCT is the prior successes[12-14,27,28] of the lattice cluster theory[11,30] in explaining the composition and temperature dependence of SANS data for polymer blends and diblock copolymer melts.

When applied to a binary polymer blend, the LCT contains four empirical parameters: three van der Waals attractive energies $\epsilon_{\alpha\beta}$ and the volume $v_{cell}^{(blend)}$ of a unit cell. Given these empirical parameters, the LCT then predicts a wide variety of blend thermodynamic properties as a function of the pressure P, temperature T, composition Φ_1, polymerization indices N_1 and N_2, and monomer structures of the two blend components. The theory is illustrated by application to PS/PVME blends and PS-*b*-PMMA diblock copolymer melts.

The self-interaction energies ϵ_{S-S} and $\epsilon_{VME-VME}$ as well as the pure component cell volumes $v_{cell}^{(PS)}$ and $v_{cell}^{(PVME)}$ are determined by fitting the LCT pure melt equation of state to *PVT* data for the pure PS and PVME melts. Our analysis of the pure component *PVT* data proceeds by using only two adjustable microscopic empirical parameters in the LCT, while prior treatments of melt equations of state generally employ three (or more) macroscopic thermodynamic parameters for each pure component. The use of only two empirical parameters for each pure component leads to a reproduction of experimental *PVT* data over modest (ca. 10^3 atm) pressure ranges, but this range more than suffices for our analysis of the pressure-dependent SANS data for blends.

A traditional method for estimating the two blend parameters ϵ_{S-VME} and $v_{cell}^{(blend)}$ is based on the use of various combining rules. Our calculations demonstrate that the standard cell volume combining rule[38] from eq 3.1 provides a useful value for v_{cell} since application of this combining rule in conjunction with the LCT yields a very good reproduction of the volume change on mixing (see Figure 10). On the other hand, the traditional combining rules for the heterocontact interaction energy ϵ_{AB}, such as the geometrical mean[39] of eq 3.2, are grossly inadequate in generating suitable values for ϵ_{S-VME}. This inadequacy stems from the extreme sensitivity of almost all blend thermodynamic properties to ϵ_{S-VME}. (See further discussion below.) The strong sensitivity to ϵ_{S-VME} also suggests the exercise of caution in extracting heterocontact interaction energies ϵ_{AB} from molecular mechanics or quantum mechanical computational methods. The ϵ_{S-VME} (and similarly ϵ_{S-MMA} for the PS-*b*-PMMA diblock copolymer system) are obtained here from fits to experimental SANS data of the LCT computations for χ_{eff}/v_0. An alternative choice would involve adjusting ϵ_{S-VME} to reproduce *PVT* data for PS/PVME blends, but unfortunately these data are not available. Figures 7a−c demonstrate that the adjustment of a single ϵ_{S-VME} parameter then enables the LCT

computations to reproduce quite satisfactorily the extensive 1 atm pressure SANS data for PS/PVME as a function of temperature and composition. The spinodal curves (see figure 8) are then calculated without the need for additional adjustable parameters as are the correlation lengths ξ (Figure 9) and the volume change on mixing ΔV (Figure 10). All three sets of the latter computed quantities are in good agreement with the experimental data of Han et al.[23] and of Shiomi et al.[42]

The plots in Figures 7–10 are evaluated for the energy parameter set $\epsilon_{S-S} = 0.62k_BT_0$, $\epsilon_{VME-VME} = 0.59k_BT_0$, and $\epsilon_{S-VME} = 0.607675k_BT_0$. The fitted value ϵ_{S-VME} differs only by about 0.5% from the geometrical mean $(\epsilon_{S-S}\epsilon_{VME-VME})^{1/2}$ used in the most common combining rule.[39] However, the phase diagrams predicted for these two almost identical values of ϵ_{S-VME} are completely different. The fitted ϵ_{S-VME} yields a LCST phase diagram, while the geometrical mean produces an UCST phase diagram. The qualitative explanation of such dissimilar phase behaviors may be understood even using simple FH theory, where the only theoretical parameter is ϵ, which completely controls the phase behavior. Since $\epsilon \equiv \epsilon_{S-S} + \epsilon_{VME-VME} - 2\epsilon_{S-VME}$ emerges as the difference between two sets of nearly identical energies $\epsilon_{S-S} + \epsilon_{VME-VME}$ and $2\epsilon_{S-VME}$, a very small alteration in ϵ_{S-VME} can easily change the sign of ϵ and, consequently, the whole predicted phase behavior.

The LCT is also able to reproduce the experimental data for the SANS effective interaction parameter χ_{eff} at $P = 1$ atm, the spinodal curves, the correlation lengths ξ, and the volume change on mixing ΔV, using another somewhat different set of self-interaction energies that have the opposite relative ordering $\epsilon_{S-S} < \epsilon_{VME-VME}$, while ϵ_{S-VME} remains similar to the fitted value given above. However, this alternative set of ϵ_{S-S} and $\epsilon_{VME-VME}$ does not reproduce the *PVT* data for pure PS and PVME melts. This second fit is quite useful for emphasizing the importance of having *PVT* data for the melts and for illustrating possible phase behaviors that may arise in other LCST polymer blends.

Our earlier description[41] for the experimental observation of PS chain expansion and PVME chain contraction (when either is a minority component in a PS/PVME blend) notes a correlation between chain expansion or contraction and differences in the attractive interaction parameters $\epsilon_{\alpha\beta}$. This correlation emerges only for the second set of parameters (with $\epsilon_{S-S} < \epsilon_{VME-VME}$) that are inadequate for describing pure melt *PVT* properties. Thus, the observed pattern of chain dimension alteration in these blends is probably governed by a more complicated mechanism involving a combination of contributions from both repulsive and attractive forces. An improved understanding of this phenomenon and many others requires the generation of reliable *PVT* data for both PS/PVME blends and their pure components. Especially important is the production of *PVT* data for low-polydispersity PVME samples that are carefully prepared to eliminate any traces of water. Ideally, the *PVT* measurements should be performed for the identical samples used in the SANS experiments, as this would automatically eliminate errors in the determination of $\epsilon_{VME-VME}$ and, hence, in the theoretical analysis of the SANS data. Nevertheless, the present computations demonstrate that the LCT operates quite well in the context of the traditional liquid mixture philosophy. The pure substance *PVT* data suffice to determine the pair of empirical parameters for each species, and a limited amount of binary blend data is adequate for providing the heterocontact interaction energy. The LCT then yields an excellent representation of the composition, temperature, and molecular weight dependence of the SANS data as well as other thermodynamic data. Our theory of binary blends involves only four adjustable parameters, whereas previous treatments use seven or eight at minimum.

While it has been customary to analyze SANS data using the assumption of blend incompressibility, we have repeatedly stressed the importance of including a description of blend compressibility (i.e., "equation of state effects") in any desire for a microscopic understanding and analysis of SANS data for blends. Indeed, the lower critical solution temperature (LCST) phase behavior of PS/PVME blends is only explained by invoking blend compressibility unless a purely phenomenological composition-dependent χ_{eff} is introduced with a plethora of empirical parameters. One consequence of this blend compressibility is evident from our previous LCT computations[12] that predict an interesting pressure dependence to the SANS χ_{eff} for blends with either upper or lower critical solution temperatures. The earlier predictions, however, could not assess whether the $\{\epsilon_{\alpha\beta}\}$ should be required to vary with pressure. The recent pressure-dependent SANS experiments for PS/PVME blends by Janssen et al. and by Hammouda and Bauer provide adequate information for resolving this question and more pertinent ones of whether the LCT can explain those new data without the introduction of additional empirical parameters. We, therefore, present extensive LCT computations for the pressure dependence of the effective interaction parameter χ_{eff} and of the absolute neutron scattering intensity $I(0)$. The latter quantity $I(0)$ is a directly measured property (apart from the extrapolation to the zero angle), and this stands in marked contrast to the description of χ_{eff}, which traditionally has involved the oversimplified assumption of blend incompressibility. The analysis of the SANS χ_{eff} is rendered more difficult because various experimental groups employ slightly different definitions of χ_{eff}, a feature that hinders the comparison of data between various experiments and with theory. Thus, we reanalyze the pressure-dependent χ_{eff} data using a common definition and analysis of χ_{eff} for the both the data of Janssen et al. and Hammouda and Bauer. Use of a common definition resolves some of the previously noted apparent discrepancies between the data of these two groups, but some differences still persist. (Further experimental studies are necessary to delineate the origins of the remaining discrepancy described below.) Nevertheless, our reanalysis of the Janssen et al. data shows that both their data and those of Hammouda and Bauer display a pressure dependence for the entropic and for the enthalpic portions of χ_{eff}/v_0. The general experimental trends are in qualitative accord with each other and with those calculated from the LCT without the introduction of additional parameters and without requiring the $\{\epsilon_{\alpha\beta}\}$ to be pressure dependent. Quantitative agreement is not possible with both sets of data because their χ_{eff}/v_0 appear to be displaced by roughly a constant shift from each other, and their $P = 1$ atm data likewise depart from the $P = 1$ atm SANS data of Han et al. (see Figure 11, for example). The observed decrease with pressure of χ_{eff} for PS/PVME blends (Figure 12) has serious thermodynamic implications. The LCST phase diagram shifts with pressure to higher temperatures. This feature suggests that the presence of excess free volume (which is more prevalent at high

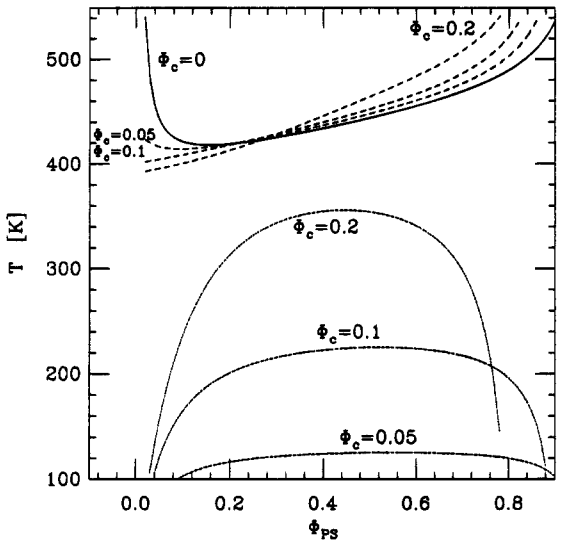

Figure 20. LCT prediction for the constant-pressure phase diagram of a ternary PS/PVME/PS-*b*-PVME system with $N_{PS} = N_{PVME} = N_{PS}^{(b)} = N_{PVME}^{(b)} = 10^3$. All the spinodal curves are obtained[31] from the vanishing of the 2 × 2 determinant of second derivatives $\partial^2 g/\partial\Phi_i\partial\Phi_j$, $i\,j = 1,2$, (where g is a specific Gibbs free energy per occupied lattice site). The spinodals are calculated for a constant amount Φ_c of the diblock component and for a constant pressure of 1 atm. The presence of diblock copolymer ($\Phi_c \neq 0$) distorts the LCST portion of the phase diagram and leads to the emergence of an UCST branch, which is very sensitive to the magnitude of Φ_c.

temperatures and low pressures) interfers with the compatibility of PS/PVME blends. More analysis should consider whether this is a common property of all blnds with a LCST. The strong pressure dependence of χ_{eff}, first predicted[12] by the LCT[11] and later confirmed experimentally, should also have important technological ramifications.

While the computations described in section III are performed mostly for binary polymer systems, we close by presenting the LCT predictions for a more complex system. Figure 20 depicts the phase diagram[31] for a ternary PS/PVME/PS-*b*-PVME mixture at constant composition Φ_c of the PS-*b*-PVME diblock copolymer and a constant pressure of 1 atm. The LCST critical temperature shifts very little upon the addition of block copolymer, but the spinodals become quite distorted from the binary blend limit as the blend composition moves away from the critical composition. More interesting is the emergence of an upper critical solution temperature branch, with the UCST critical temperature sensitive to the amount of added diblock copolymer. On the other hand, LCT calculations with a somewhat different set of interaction energies produce qualitatively different trends. When the self-interaction energies have the opposite relative ordering $\epsilon_{S-S} < \epsilon_{VME-VME}$, the LCT computations predict a hugh destabilization[31] (not shown) of PS/PVME blends at very low concentrations of diblocks (Φ_c order of 10^{-4}). It is reasonable to anticipate the existence of actual binary blends exhibiting either ordering of the self-interaction energies. The generation of *PVT* data for PS/PVME blends and the availability of more extensive *PVT* data for PVME melts would be useful in determining whether further adjustments are necessary in the interaction energy parameters since slight changes in their values strongly affect the phase diagrams for PS/PVME/PS-*b*-PVME mixtures.

Acknowledgment. This research is supported, in part, by NSF DMR Grant No. 92-23804. We thank Stefan Janssen, Dietmar Schwahn, Boualem Hammouda, and Charles Han for useful discussions and Greg Dee for providing us the PVT data for pure PS and PVME melts.

References and Notes

(1) Flory, P. J. *Principles of Polymer Chemistry*; Cornell University Press: Ithaca, NY, 1953.
(2) Dudowicz, J.; Freed, K. F.; Madden, W. G. *Macromolecules* **1990**, *23*, 4803. Falsafi, A.; Madden, W. G. *Macromolecules* **1994**, *27*, 3094.
(3) Sariban, A.; Binder, K. *J. Chem. Phys.* **1987**, *86*, 5859. Dickman, R.; Hall, C. K. *J. Chem. Phys.* **1986**, *85*, 3023.
(4) Baumgartner, A. In *Applications of the Monte Carlo Methods in Statistical Physics*; Binder, K., Ed.; Springer: Berlin, 1984; Chapter 5. Binder, K.; Heermann, D. W. *Monte Carlo Simulation in Statistical Physics: An Introduction*; Springer: Berlin, 1988.
(5) Dickman, R.; Hall, C. K. *J. Chem. Phys.* **1986**, *85*, 4108.
(6) Schweizer, K. S.; Curro, J. G. *Adv. Polym. Sci.* **1994**, *116*, 319; *J. Chem. Phys.* **1989**, *91*, 5059.
(7) Lipson, J. E. G. *Macromolecules* **1991**, *24*, 1334; *J. Chem. Phys.* **1992**, *96*, 1418. Taylor, M. P.; Lipson, J. E. G. *J. Chem. Phys.* **1992**, *97*, 4301. Sevian, H. M.; Brazhnik, P. K.; Lipson, J. E. G. *J. Chem. Phys.* **1993**, *99*, 4112.
(8) Freed, K. F. *J. Phys. A* **1985**, *18*, 871.
(9) Nemirovksy, A. M.; Bawendi, M. G.; Freed, K. F. *J. Chem. Phys.* **1987**, *87*, 7272.
(10) Freed, K. F.; Bawendi, M. G. *J. Phys. Chem.* **1989**, *93*, 2194.
(11) Dudowicz, J.; Freed, K. F. *Macromolecules* **1991**, *24*, 5074.
(12) Dudowicz, J.; Freed, M. S.; Freed, K. F. *Macromolecules* **1991**, *24*, 5096.
(13) Dudowicz, J.; Freed, K. F. *Macromolecules* **1991**, *24*, 5112.
(14) Freed, K. F.; Dudowicz, J. *Theor. Chim. Acta* **1992**, *82*, 357.
(15) Schweizer, K. S. *Macromolecules* **1993**, *26*, 6033. Kumar, S. K. *Macromolecules* **1994**, *27*, 260.
(16) Janssen, S.; Schwahn, D.; Mortensen, K.; Springer, T. *Macromolecules* **1993**, *26*, 5587.
(17) Hammouda, B.; Bauer, B. J. *Macromolecules* **1995**, *28*, 4505.
(18) Dee, G. T.; Walsh, D. J. *Macromolecules* **1988**, *21*, 811, 815.
(19) Sanchez, I. C.; Lacombe, R. H. *Macromolecules* **1978**, *11*, 1145. Lipson, J. E. G.; Andrews, S. S. *J. Chem. Phys.* **1992**, *96*, 1426.
(20) Krishnamoorti, R.; Graessley, W. W.; Dee, G. T.; Walsh, D. J.; Fetters, L. J.; Lohse, D. J., preprint.
(21) Sanchez, I. C.; Balazs, A. *Macromolecules* **1989**, *22*, 2325.
(22) After the present paper was submitted for publication, a paper by Bidkar and Sanchez appeared in *Macromolecules* (*Macromolecules* **1995**, *28*, 3973), and we have received a preprint from Taylor, Debenedetti, Graessley, and Kumar. Both apply the lattice fluid model to SANS data, using three parameters for each pure component and one more for a binary interaction parameter, giving seven parameters for a binary blend.
(23) Han, C. C.; Bauer, B. J.; Clark, J. C.; Muroga, Y.; Matsushita, Y.; Okada, M.; Tran-cong, Q.; Chang, T.; Sanchez, I. C. *Polymer* **1988**, *29*, 2002.
(24) Ougizawa, T.; Dee, G. T.; Walsh, D. J. *Polymer* **1989**, *30*, 1675.
(25) Russell, T. P.; Hjem, R. P., Jr.; Seeger, P. A. *Macromolecules* **1990**, *23*, 890.
(26) Russell, T. P., private communication.
(27) Freed, K. F.; Dudowicz, J. *J. Chem. Phys.* **1992**, *97*, 2105.
(28) Dudowicz, J.; Freed, K. F. *Macromolecules* **1993**, *26*, 213.
(29) Freed, K. F. *J. Chem. Phys.* **1988**, *88*, 5871. Dudowicz, J.; Freed, K. F. *Macromolecules* **1990**, *23*, 1519.
(30) Dudowicz, J.; Freed, K. F. *J. Chem. Phys.* **1993**, *100*, 4653.
(31) Dudowicz, J.; Freed, K. F.; Douglas, J. F. *Macromolecules* **1995**, *28*, 2276.
(32) The coefficients f_j for a pure homopolymer melt are summarized in Table 1 of ref 12 and denoted there as g_{av}, while the f_j for a diblock copolymer system may be easily obtained from Tables 1 and 2 of ref 30 by collecting the contributions with the same powers of ϕ. The binary polymer blend coefficients f_{ij} follow, after performing simple algebra, from the polynomials in Tables 1 and 2 of ref 11, with some corrections presented in footnote 32 of ref 31. The latter tables also apply to multicomponent systems, with one or more of the components possibly small molecules. The f_j and f_{ij} in these tables depend on a set of combinatorial indices associated with the monomer structures, which are provided for a variety of monomer architectures in Table 1 of refs 9

and 13. While it is straightforward to program and process these expressions, an alternative to programming the free energy expressions is to contact the authors for use of their computer codes.
(33) de Gennes, P.-G. *Scaling Concepts in Polymer Physics*; Cornell University Press: Ithaca, NY, 1979.
(34) Kohler, F. *The Liquid State*; Verlag Chemie: Weinheim/ Bergstr, 1972. Higgins, J.; Benoit, H. *Polymers and Neutron Scattering*; Oxford University Press, New York, 1994.
(35) Hill, T. L. *Statistical Mechanics*; McGraw-Hill: New York, 1956. Hansen, J. P.; MacDonald, I. R. *Theory of Simple Liquids*; Academic Press: New York, 1986.
(36) Liebler, L. *Macromolecules* **1980**, *13*, 1602.
(37) Tang, H.; Freed, K. F. *Macromolecules* **1991**, *24*, 958.
(38) Hamada, F.; Shiomi, T.; Fujisawa, K.; Nakajima, A. *Macromolecules* **1980**, *13*, 729. Shiomi, T.; Fujisawa, K.; Hamada, F.; Nakajima, A. *J. Chem. Soc., Faraday Trans. 1* **180**, *76*, 885. Fujisawa, K.; Shiomi, T.; Hamada, F.; Nakajima, A. *Polym. Bull.* **1980**, *3*, 261.
(39) Rowlinson, J. S.; Swinton, F. L. *Liquids and Liquid Mixtures*, 3rd ed.; Butterworths: London, 1982.
(40) Dudowicz, J.; Freed, K. F. *J. Chem. Phys.* **1992**, *96*, 9147.
(41) Dudowicz, J.; Freed, K. F. *J. Chem. Phys.* **1992**, *96*, 1644.
(42) Shiomi, T.; Hamada, F.; Nasako, T.; Yoneda, K.; Imai, K.; Nakajima, A. *Macromolecules* **1990**, *23*, 229.
(43) An alternative model for deriving a nontrivial equation of state proceeds by allowing the volume associated with a single lattice site to be a function of the pressure. However, this approach is not employed here since its use requires several more adjustable parameters.
(44) *Polymer Handbook*; Brandup, J., Immergut, E. H., Eds.; Wiley: New York, 1989.

MA950360K